GRAPHLETS AS BUILDING BLOCKS FOR STRUCTURAL VOCABULARY IN GRAPH FOUNDATION MODELS

Anonymous authors
Paper under double-blind review

ABSTRACT

Foundation models excel at language, where sentences become tokens, and vision, where images become pixels, because both reduce to discrete symbols on a shared, fixed grid. Knowledge Graphs share the discreteness, but not the geometry. Their entities and relations are discrete symbols, yet their arrangement is relational and lacks a common, fixed grid. Knowledge Graphs (KGs) share the discreteness, but not the geometry. They form irregular, non-Euclidean topologies whose local neighborhoods differ from graph to graph. Therefore, Knowledge Graph Foundation Models (KGFMs) rely on identifying structural invariances to produce transferable representations. Without a universal token set, KGFMs are limited in their ability to transfer representations across unseen KGs. We close this gap by treating graphlets, small connected graphs, as structural tokens that recur in heterogeneous KGs. In this paper, We introduce a model-agnostic framework based on a vocabulary of graphlets that mines a KG between relations via pattern matching. In particular, we considered closed and open 2- and 3-path, and star graphlets, to obtain robust invariances. The framework is evaluated on 51 KGs from a wide range of domains, for zero-shot inductive and transductive link prediction. Experiments show that adding simple graphlets to the vocabulary yields models that outperform prior KGFMs. Our code is available at: https://anonymous.4open.science/r/ultra-augmentations/

1 INTRODUCTION

Recently, Large language Models (LLMs), have garnered significant attention for their remarkable natural language understanding capabilities (Bommasani, 2021; Zhao et al.; Wei et al., 2022). These models are pretrained on massive corpora of diverse text data (Chang et al., 2024), allowing them to learn not only the syntax and grammar of language but also the semantics and contextual usage of words and phrases. Despite differences in architecture (e.g., transformer-based, decoder-only, encoder-decoder), all LLMs operate on tokens; basic units of text that may be whole words or subwords. During training, the models construct a universal vocabulary of tokens. This token-based processing enables LLMs to generalize effectively to new words by breaking them down into familiar token components. In turn, complete sentences can be reconstructed from these tokens. As a result, LLMs achieve strong generalization across languages (Lin et al., 2021), domains (Pan et al., 2024), and (Brown et al., 2020; Wang et al., 2022). The (unstructured) textual data can be saved as tripled-based data, known as Knowledge Graphs (Hogan et al., 2021; Noy et al., 2019; Ehrlinger & Wöß, 2016). Knowledge Graph embeddings (KGEs) are a class of representation learning models specialized for Knowledge Graphs (KGs). They learn entity and relation embeddings based on their labeled identities and the structure of the triples they participate in (Wang et al., 2017). While effective at modeling relational patterns, they are limited in their ability to generalize to unseen entities or relations.

In contrast to LLMs, KGEs do not capture any natural understanding of the labels themselves. As a result, adapting KGEs to new entities or relation types typically requires retraining from scratch on augmented data (Hamaguchi et al., 2017; Teru et al., 2020). To overcome this limitation, recent approaches explore structure-driven generalization in (Liu et al., 2021). One idea is to treat structural patterns in a graph analogously to how LLMs treat tokens in text data. These patterns capture local and global structural invariants independent of specific entity labels or relation types.

Motivating Example. Let us consider the three illustrative KGs: Family, Corporate and Scholarly, shown in Figure 1. Despite the fact that the type of relations and entity labels are not the same, their underlying structural topology is the same. This allows for a mapping between their rela-

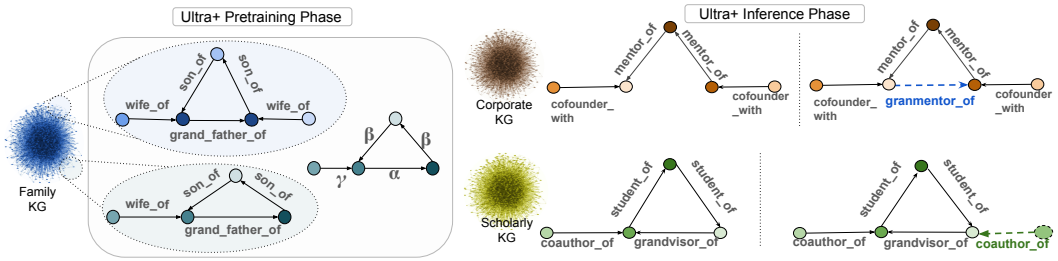

Figure 1: The KGFM model Ultra$^+$, pretrained on a large collection of KGs, including the Family KG, recognizes the Corporate, and Academic KGs as instances of the same graphlet patterns.

tions (*grand_father_of* $\leftrightarrow$ *grandvisor*, *son_of* $\leftrightarrow$ *mentor_of*, *wife_of* $\leftrightarrow$ *cofounder_with*) enabling structure-level transfer. This core insight forms the basis of KGFMs. Rather than embedding labels, KGFMS (Galkin et al., Huang et al.) learn to reason over vocabulary of relations forming relational subgraphs. Group of ordered relations that co-occur within a specific type of subgraph is referred to as an occurrence of a graphlet. These graphlets form the core of the structural vocabulary used to construct a relation graph, where relations become nodes, and the graphlets define typed edges between them. As shown in Figure 1, a KGFM would detect and save the pattern formed by the cycle $(\gamma, \alpha, \beta, \beta)$ as part of its vocabulary. This learned pattern can then be used to infer missing facts such as the triple *mentor_of*(A. Einstein, ?). However, existing KGFMs have limitations. First, they fail to distinguish between closed and open paths, treating all subgraphs of similar size as equally informative. Second, a single occurrence of a graphlet is often enough to connect involved relations in the relation graph, which may lead to decreased robustness.

Our Contributions. The key contributions of our model Ultra$^+$ are as follows

(i) **Query-based relation graph extraction**: We propose a flexible SPARQL-based extraction method that efficiently identifies informative structures without relying on sparse matrix multiplication (SPMM);

(ii) **Closed and open relations**: We incorporate both closed and open graphlets to capture a wider range of relational patterns;

(iii) **Binary relation**: We represent graphlets as positional binary relations than traditional n-ary relations; and

(iv) **Model-agnostic design**: Ultra+ is modular and can be integrated into any KGFM that uses relation graphs or structural vocabulary, making it adaptable across KGFM architectures.

Ultra$^+$ substantially strengthens how KGFMs capture and represent complex structural patterns. Its main objective is not to propose a new model architecture, but to boost performance and create more robust KGFMs by enriching their structural vocabulary.

2 Related Work

A KGE model learns the vector representations of relations ($\mathbf{r}$) and entities ($\mathbf{E}$) of KGs via parametrized relation-specific transformation functions, $\Phi_{\mathbf{r}} : \mathbf{h} \mapsto \Phi_{\mathbf{r}}(\mathbf{h})$, over the entity embedding space. KGEs can be categorized based on their underlying principles such as geometric transformations, tensor decomposition, deep neural architectures, or foundational graph approaches.

Geometric and Tensor Decomposition Models. These models can be grouped into three main types. The first are translational-based models such as TransE (Bordes et al., 2013) , TransH (Wang et al., 2014), and TransR (Lin et al., 2015), which embed entities and relations in real vector space and use identity mappings ($\Phi_{\mathbf{r}} = \mathbf{r}$). TransH and TransR add extra relation embeddings, to improve modeling capacity. While effective for link prediction, these models struggle with relational patterns like closed paths. To address these limitations, rotation-based models such as RotatE (Sun et al., 2019) were introduced. RotatE represents relations as rotations: $\Phi_{\mathbf{r}}(\mathbf{h}) = e^{i\theta_r}\mathbf{h}$ with $\theta_r \in (-\pi, \pi]^d$.

This shift from real to complex algebra enables better modeling of relational patterns. However, these models are not generalizable to new entities and relations.

Deep Neural Network Models. These models leverage deep learning to extract graph representations. A primary category includes Graph Neural Networks (GNNs), especially graph convolutional models that iteratively aggregate information from neighboring nodes. A pioneer work is Relational GNC (Schlichtkrull et al., 2018), an encoder-decoder model. The encoder of R-GCN learned latent embedding of entities, which are passed to the decoder based on DistMult, a tensor decomposition model. However, R-GCNs does not learn relation embeddings. To address this limitation, TransGCN, RotatEGCN (Cai et al., 2019), and ComplexGCN (Zeb et al., 2022) integrate GCNs with geometric KGE models like TransE, RotatE, and ComplEx to jointly learn entity and relation embeddings and capture richer structural semantics. End-to-end trainable GNNs are restricted to a single KG downstream task and cannot generalize to new KGs without retraining.

Knowledge Graph Foundation Models. KGFMs overcome these limitations by enabling pretrained GNNs or LLMs to inductively generalize to new KGs in zero or few-shot paradigms (Wang et al., 2025; Liu et al., 2023). ULTRA (Galkin et al., 2023), a KGFM for KG reasoning, constructs a relation graph whose nodes are the relations from the original KG, and edges represent the connections between relations in paths of length two. Leveraging on the invariance of relational structure across datasets, a labeling trick, and conditional representations on both relations and entities, Ultra enhances the generalization of KG reasoning. ULTRAQuery (Galkin et al., 2024) exploits the ability of Ultra in KG reasoning to find potential missing links, and uses non-parametric fuzzy logic operators to answer complex questions. AnyGraph (Xia & Huang, 2024) overcomes the limit of Ultra, by generalizing to in- and cross- domain link prediction, and node and graph classification tasks. The key factor behind the success of existing KGFMs lies in the construction of suitable graph vocabularies (Mao et al., 2024), i.e. basic transferable units that underlie graphs. While models such as Mole-BERT relies on context-aware atom vocabulary (Xia et al., 2023) for molecule graph classification, Ultra and Motif (Huang et al., 2025) rely on paths of length two and motifs to define graph vocabulary, respectively. However, these approaches overlook closed paths, which are prevalent and essential.

In this paper, we extend the Ultra framework by introducing a novel graphlet-based vocabulary for KG reasoning. Unlike Ultra, our framework explicitly encodes cyclic structures, this allows us to capture richer structural patterns beyond simple paths of length two. Moreover, in contrast to Motif, our vocabulary supports higher-order interaction patterns via binary relations within a standard relation graph, rather than relying on n-ary relations in a relation hypergraph. This ensures our relation graph remains a simple KG, preserving compatibility with most established KG processing techniques.

3 PRELIMINARIES

3.1 INDUCTIVE KNOWLEDGE GRAPH EMBEDDINGS

We consider a *Knowledge Graph* as a multi-relational directed graph $K = (\mathcal{E}^K, \mathcal{R}^K, \mathcal{T}_+^K)$ where $\mathcal{E}^K, \mathcal{R}^K$, and $\mathcal{T}_+^K$ are the set of nodes (entities), edge labels (relations), and ordered pairs (edges or triples) formed as *relation(head entity, tail entity)* respectively. We refer to the head and tail entity as h and t or e in general, and to the relation as r or q. $\mathcal{T}_+^K$ is a subset of $\mathcal{T}^K$ which contains all plausible triples; and $\mathcal{T}_-^K = \mathcal{T}^K \setminus \mathcal{T}_+^K$ is the set of corrupted triples. Since all entities in $\mathcal{E}^K$ are used in constructing $\mathcal{T}_+^K$, corrupted triples (used as negative samples) result from replacing the head or the tail entity of true triples. The set $\mathcal{N}(r,t) = \{h | r(h,t) \in \mathcal{T}^+\}$ is called the neighborhood of t.

A *relation graph* is constructed from the KG by examining how relations within a target KG appear collectively in subgraphs. The labels on its edges and nodes originate from subgraph configurations and relations within the target KG. The relations in a relation graph can also be referred to as *meta-relations* (see Section 4.1 for more details).

KGE models pretrained on K are evaluated on a test KG $K_{test} = (\mathcal{E}_{test}^K, \mathcal{R}_{test}^K, \mathcal{T}_{test+}^K)$ to predict missing links. Entities in $\mathcal{E}_{test}^K \setminus \mathcal{E}^K$ and relations in $\mathcal{R}_{test}^K \setminus \mathcal{R}^K$ are called unseen entities and relations, respectively. A KGE model is a *transductive* model if $\mathcal{E}_{test}^K \subseteq \mathcal{E}^K$ and $\mathcal{R}_{test}^K \subseteq \mathcal{R}^K$, an *inductive* model otherwise. *Zero-Shot Link Prediction* (ZSLP) involves evaluating models pretrained on K, directly on K_{test}. Inductive ZSLP can be categorized into three main tasks: *Relation learning* involving predicting unseen relations (Ind.(r)), *entity learning* focusing on predicting facts involving

unseen entities (Ind.(e)), and *graph transfer* requiring generalization to both unseen entities and relations (Ind.(e,r)).

3.2 KNOWLEDGE GRAPH HOMOMORPHISM

A key feature of our framework is its ability to detect occurrences of specific subgraph patterns within a KG by leveraging graph homomorphisms for structural matching.

A *KG homomorphism* is a structure preserving mapping between two KGs. It consists of entity and relation mappings to relate entities and relations from one KG to the other. Thus, $\phi : K \to K'$ is a KG homomorphism if there exists two mappings $\eta : \mathcal{E}^K \to \mathcal{E}^{K'}$ and $\rho : \mathcal{R}^K \to \mathcal{R}^{K'}$ so that the product function $\eta \cdot \rho \cdot \eta$ maps any triple $r(h,t) \in \mathcal{T}^K$ to $\phi(r(h,t)) = \rho(r)(\eta(h), \eta(t)) \in \mathcal{T}^{K'}$. $\phi(K) = \big(\eta(\mathcal{E}^K), \rho(\mathcal{R}^K), \phi(\mathcal{T}^K)\big)$, the *image KG* of K by ϕ, is a subgraph of K'. A homomorphism ϕ is said to be *injective* if η and ρ are both injective. An injective KG homomorphism ϕ is called *KG monomorphism* and its mapping is represented by $\phi : K \xrightarrow{mon} K'$.

3.3 GRAPHLETS AND MOTIFS

The objective of our proposed method is to represent relational invariances and develop a structural vocabulary. To this end, the method identifies different graphlet occurrences within a KG. Usually graphlets are defined as induced subgraphs with respect to a Knowledge Graph while motifs are graphlets that occur frequently in a given KG (Pržulj, 2007; Milo et al., 2002; Ribeiro et al., 2021). To represent relational patterns in a more nuanced way, the following definitions are employed.

Definition 3.1 (Graphlet)**.** A graphlet $\mathcal{G} = (G, \mathrm{g})$ is a (small) connected Knowledge Graph $G = (\mathcal{E}, \mathcal{R}, \mathcal{T})$ with an order g on $\mathcal{R}$. $\mathrm{g}(\mathcal{R}) = \mathrm{g}\,(r_1, r_2, \ldots, r_m)$ a tuple defining the order on $\mathcal{R} \ni r_i$. The cardinality of a graphlet $\mathcal{G}$ is the number of its edges, $card(\mathcal{G}) = |\mathcal{T}|$.

The order specifies the manner in which directed relations within $\mathcal{R}$ connect their endpoints to create the graph structure. The order can relate two or many relations in $\mathcal{R}$; it is called *binary* and *n-ary* respectively. The arity (n) can be reduced from n to m with $m \leq n$ by only considering m relations as arguments and the $n - m$ remaining relations become dummy arguments. This order is referred to as a *positional m-ary order*; it is denoted by $\mathrm{g}_{i_1,\ldots,i_m \leq n}$ when the attention is to stress on the position of the arguments and the initial arity. Thus $\mathrm{g}_{1,2,3\leq 3}$ is an ordinary 3-ary order whereas $\mathrm{g}_{1,3\leq 3}$ is a positional binary order.

Theorem 3.2. *Any positional m-ary order, $m < n$, spans a group of n-ary orders.*

In particular, the tuple $\mathrm{g}_{1,3\leq 3}(\mathcal{R})$ could be induced by any of $\mathrm{g}_{1,1,3}(\mathcal{R}), \mathrm{g}_{1,3,3}(\mathcal{R})$ and $\mathrm{g}_{1,2,3}(\mathcal{R})$. In other words, if $\mathrm{g}_{1,3\leq 3}(\mathcal{R})$ does not exist, then neither $\mathrm{g}_{1,1,3}(\mathcal{R}), \mathrm{g}_{1,3,3}(\mathcal{R})$ nor $\mathrm{g}_{1,2,3}(\mathcal{R})$ exist.

Definition 3.3 (Graphlet occurrence)**.** Let $K = (\mathcal{E}^K, \mathcal{R}^K, \mathcal{T}^K)$ be a KG, and g a positional m-aray order. A graphlet $\mathcal{G} = (G, \mathrm{g})$ *occurs* in K if and only if G is monomorphic to K, and the monomorphism $\phi_{\mathrm{g}} : G \xrightarrow{mon} K$ is an order-preserving mapping; that is, ρ maps $\mathrm{g}(\mathcal{R})$ to $\mathrm{g} \circ \rho(\mathcal{R}) = \mathrm{g}\,(\rho(r_1), \rho(r_2), \ldots, \rho(r_m))$. The tuple $\mathrm{g}(\mathcal{R})$ induces the set of tuples $\mathrm{g}(\mathcal{R}^K) = \Big\{\mathrm{g} \circ \rho(\mathcal{R}) | \rho : \mathcal{R} \xrightarrow{mon} \mathcal{R}^K\Big\}$. The image graph $\phi_{\mathrm{g}}(G)$, is called an *occurrence* of $\mathcal{G}$ in K. The set of occurrences of $\mathcal{G}$ in K is denoted and defined by $\mathcal{G}(K) = \Big\{\phi_{\mathrm{g}}(G) | \phi_{\mathrm{g}} : G \xrightarrow{mon} K\Big\}$. Two occurring subgraphs $\phi(G)$ and $\phi'(G)$ are said *equivalent*, $\phi(G) \equiv_{\mathrm{g}} \phi'(G)$, if $\rho(r_{i_j}) = \rho'(r_{i_j})$ for $j \leq m, i_j \leq n$, and $r_{i_j} \in \mathcal{R}$. The equivalence class denoted by $\overline{\phi(G)} = \{\phi'(G) | \phi'(G) \equiv_{\mathrm{g}} \phi(G)\}$ is the set of subgraph occurrences equivalent to $\phi(G)$ and $\overline{\mathcal{G}(K)} = \Big\{\overline{\phi(G)} | \phi(G) \in \mathcal{G}(K)\Big\}$ is the set of all equivalence classes.

The fact that two classes $\overline{\phi(G)}$ and $\overline{\phi'(G)}$ are different if and only if $\rho(\mathcal{R}) \neq \rho'(\mathcal{R})$ implies that there is a one-to-one correspondence between $\overline{\mathcal{G}(K)}$ and $\mathrm{g}(\mathcal{R}^K)$. We can therefore represent an equivalence class by the class $\overline{\phi(G)}$ or the tuple $\mathrm{g} \circ \rho(\mathcal{R})$.

The set of all graphlets of cardinality less than four is displayed in Figure 2. Graphlets play the role of the smallest structural entity in a Graph and are therefore well suited to investigate the local and global structure of a KG.

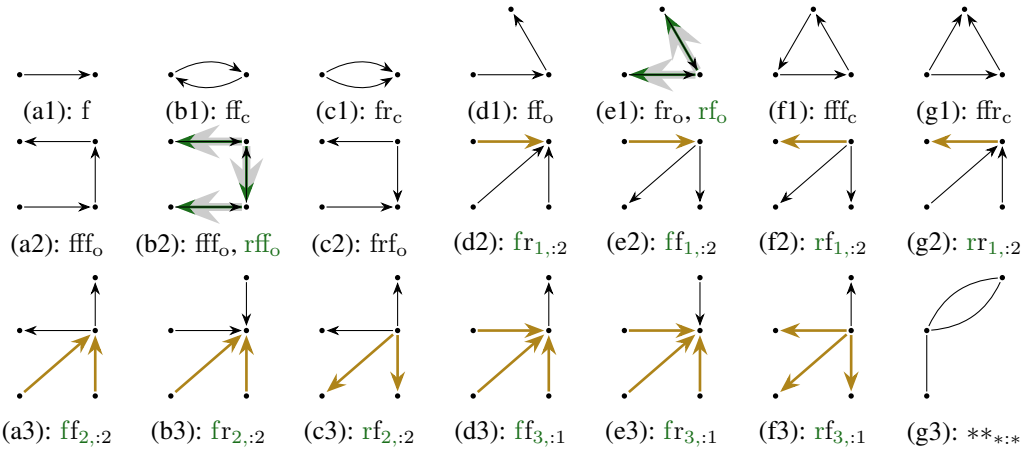

Figure 2: **Graphlets of size less than 5.** f and r denote forward and reverse edges, and subscripts c and o indicate closed and open paths. The green head arrows (shown with a light gray halo for clarity) form alternative graphlets, which are also indicated by the green labels to the right of the black text labels. The golden arrows, together with the black arrows, form distinct topological graphlets. Each vertex is marked with a small filled node for readability. The last four graphlets shown in the third column are not included in our approach.

4 METHOD

Our model Ultra$^+$ is a generalized extension of the Ultra framework introduced by Galkin et al., advancing its capabilities in relational pattern learning for KG reasoning. While the original Ultra relies solely on length-2 paths to define relational dependencies, Ultra$^+$ extends this approach by incorporating a richer set of graphlet-based patterns, capturing more complex and higher-order interactions between relations. In contrast to Motif, Ultra$^+$ constructs a binary relation graph using graphlets induced by positional binary orders, thereby preserving pairwise semantics. This shift allows Ultra$^+$ to encode cycles and subgraph patterns without resorting to hypergraph complexity.

4.1 A STRUCTURAL VOCABULARY FOR KNOWLEDGE GRAPH FOUNDATION MODELS

The structural vocabulary used to construct the relation graph constitutes the fundamental basis of Ultra$^+$.

Definition 4.1. A structural vocabulary over a KG, K, is a finite set $\mathcal{V} = \{(G_i, \mathrm{g}_i), i \leq n_V\}$ of graphlets, and a weighting function

$$\omega : \bigcup_i \overline{\mathcal{G}_i(K)} \to \mathbb{N}, \quad \overline{\phi_{\mathrm{g}}(G)} \mapsto |\overline{\phi_{\mathrm{g}}(G)}| \tag{1}$$

mapping equivalence classes of occurrences to their cardinalities. The Knowledge Graph K can be a union of KGs, that is $K = \cup_k(\mathcal{E}^k, \mathcal{R}^k, \mathcal{T}^k)$, and the domain of ω becomes $\bigcup_{i,k} \overline{\mathcal{G}_i(K_k)}$.

Definition 4.2. Let $K = (\mathcal{E}^K, \mathcal{R}^K, \mathcal{T}^K)$ be a KG, and $\mathcal{V}$ a structural vocabulary over K. We denote the *relation graph* over K upon the structural vocabulary $\mathcal{V}$ by $\mathfrak{K} = (\mathfrak{E}, \mathfrak{R}, \mathfrak{T})$ where the set of nodes $\mathfrak{E} = \mathcal{R}^K$ and meta-relations $\mathfrak{R} = \mathcal{V}$.

A structural vocabulary of binary orders yields relation graphs; conversely, relation hypergraphs are generated. The (hyper)edges in $\mathfrak{T}$ are the tuples $\mathrm{g}_i \circ \rho(\mathcal{R})$. The tuple $\mathrm{g} \circ \rho(\mathcal{R})$ does not exist unless its weight is nonzero. We say g is an ε-edge between the relations $\rho(r_1), \cdots, \rho(r_m) \in \mathcal{R}^K$, if and only if $\omega(\mathrm{g} \circ \rho(\mathcal{R})) = \varepsilon$. To define the structural vocabulary, we did not specify any graphlet. This ensures that our framework can accommodate any type of graphlet. Ultra$^+$'s structural vocabulary is restricted to (short) path and topology based vocabularies.

Path-Based Vocabulary. In a graph, K, a path of length p, $\mathcal{P}_p = \{r_i(e_i, e_i'), i = 1, \cdots, p\}$ is a subset of $\mathcal{T}^K$ such that two consecutive triples share one entity. These paths are occurrences of the nine

graphlets shown in Figures 2(b1–c2). We shall note that $\mathrm{rr_o}(r_1, r_2) = \{r_1(e_2, e_1), r_2(e_3, e_2) \in \mathcal{T}^K\}$ = $\mathrm{ff_o}(r_2, r_1)$. That is, $\mathrm{rr_o}$ can be substituted by $\mathrm{ff_o}$. In summary, the $\mathcal{P}_2$-based vocabulary $\mathcal{V}_2 = \{\mathrm{ff_{o,c}}, \mathrm{fr_{o,c}}, \mathrm{rf_o}\}$ is sufficient to characterize all closed or open 2-paths in K. In general, we define two distinct families of $\mathcal{P}_p$-based vocabularies $\mathcal{V}_p = \{\mathrm{u}_\smile\mathrm{v_z} | \mathrm{u}, \mathrm{v} \in \{\mathrm{f}, \mathrm{r}\}, \smile \in \{\mathrm{f}, \mathrm{r}\}^i, i = 0, \ldots, p-2, \mathrm{z} \in \{\mathrm{o}, \mathrm{c}\}\}$ and $\mathcal{U}_p = \{\mathrm{u}_\smile\mathrm{v} | \mathrm{u}, \mathrm{v} \in \{\mathrm{f}, \mathrm{r}\}, \smile \in \{\mathrm{f}, \mathrm{r}\}^i, i = 0, \ldots, p-2, \}$. $\smile$ is any sequence of length i over the alphabets f, r. $\mathrm{u}_\smile\mathrm{v_z}$ are positional binary orders relating the first and last relations appearing in a path of length $p > 1$. For $p = 2, \mathrm{u}_\smile\mathrm{v_z} = \mathrm{uv_z}$ and for $p = 3$, $\mathrm{u}_\smile\mathrm{w_z} := \mathrm{uvw_z} \in \{\mathrm{fff_z}, \mathrm{ffr_z}, \mathrm{frf_z}, \mathrm{rff_z} | \mathrm{z} \in \{\mathrm{o}, \mathrm{c}\}\}$. It follows that $\mathcal{V}_m \subset \mathcal{V}_n$ if $m \leq n$. This remains valid for the $\mathcal{U}_m$. It is imperative to note that the $\mathrm{u}_\smile\mathrm{v}$ positional binary orders are incapable of discerning between closed and open paths. We designed variants of Ultra^+ using these two families of structural vocabularies.

Topology-based Vocabulary. The degree of an entity in a KG is the sum of incoming and outgoing relations. The average number of degree per entity informs on the sparsity or density of the KGs. The type of relations surrounding an entity allow us to extract a subgraph centered on that entity, called an *m-star*, where m is the degree of that entity. These m-stars are occurrences of graphlets that form the topology based vocabulary, denoted by $\mathcal{M}_m$. In m-stars, we count how many times each relation appears around the centered entity. For two relations, we have $i + j = m > 2$ and any of the relation can be an ingoing or outgoing relation. We write $\mathcal{M}_{ij}$, to emphasize on the degree of the relations. Figure 2 depicts $\mathcal{M}_{12} = \{uv_{1:2} \mid u, v \{f, r\}\} = \mathcal{M}_{21} = \mathcal{M}_3, \mathcal{M}'_4 = \mathcal{M}_3 \cup \mathcal{M}_{22}$ and $\mathcal{M}_4 = \mathcal{M}_3 \cup \mathcal{M}'_4$. We combined the $\mathcal{V}_2$ and the $\mathcal{V}_3$ with the $\mathcal{M}'_4$ vocabularies to design two variants of Ultra^+.

4.2 Representation Learning

KG representation learning consists of learning the entity and relation embeddings while preserving the KG structure. In our context, relations in $\mathcal{R}$ are entities in $\mathfrak{R}$. This duality leads to two representations, as described below.

Relation Embedding. Ultra^+ embeds relations (nodes of the relation graph $\mathfrak{K}$) into d_L dimensional real vectors, $\mathbf{h}^{(L)}_{r|q}$, by an L-layer message passing GNN, $GNN_{\mathcal{G}}$. Following (Galkin et al., 2023), Ultra^+ conditioned $(r|q)$ the embedding of relations r on the query triple $q(h, ?)$. The input layer is initialized to $\mathbf{h}^{(0)}_{r|q} = \delta_{r=q}\mathbf{1}^{d_0}$, where $\delta_{r=q} = 1$ if $r = q$, and 0 otherwise. The following iterative process defines how the upcoming layers compute the embeddings

$$\mathbf{h}^{(t+1)}_{r|q} = \mathrm{UP}\big(\mathbf{h}^{(t)}_{r|q}, \mathrm{AGG}\big[\big\{\mathrm{MSG}\big(\big\{\big(\mathbf{h}^{(t)}_{r'|q}, \mathbf{u}_\smile\mathbf{v_z}\big) | r' \in \mathcal{N}(\mathrm{u}_\smile\mathrm{v_z}, \mathrm{r}), u_\smile v_z \in \mathcal{V}\big\}\big)\big\}\big]\big)$$

so that $\mathbf{R}_{|q} = GNN_{\mathcal{G}}\left(\Theta_u, \Theta_a, \Theta_m, q, \mathfrak{R}\right) \in \mathbb{R}^{|\mathcal{R}| \times d_L}$ is the conditional relation embedding matrix of all relations in $\mathfrak{E}$. UP, AGG and MSG are *update, aggregation, and message passing functions* and $\Theta_{\mathrm{x}}, \mathrm{x} = \mathrm{u}, \mathrm{a}, \mathrm{m}$ are their respective parameters.

Entity Embedding. Entities are first initialized conditionally to the query $q(h, ?)$ and the relation embedding $\mathbf{q}$, a vector column of $\mathbf{R}_{|q}$. We iteratively embed entities as follows

$$\begin{aligned}
\mathbf{h}^{(0)}_{e|h,q} &= \delta_{e=h}\mathbf{q} \\
\mathbf{h}^{(t+1)}_{e|h,q} &= \mathrm{UP}\big(\mathbf{h}^{(t)}_{e|h,q}, \mathrm{AGG}\big[\big\{\mathrm{MSG}\big(\big\{\big(\mathbf{h}^{(t)}_{e'|h,q}, \mathrm{f}^t(\mathbf{q})\big) | e' \in \mathcal{N}(r, e), r \in \mathcal{R}\big\}\big)\big\}\big]\big) \\
\pi\left(h, q, e\right) &= \mathbf{w}^\top\big(\mathbf{W}^{L'}\mathbf{h}^{(L')}_{e|h,q} + \mathbf{b}^{L'}\big) + b.
\end{aligned}$$

Motivated by the ability of geometric KGEs to capture complex relational patterns through algebraic transformations, the message-passing function is enriched with non-linear layer-specific relational transformations f^t. The transformations, $\mathrm{f}^t(\mathbf{q}) = \mathbf{W}^t_2\mathrm{ReLU}\left(\mathbf{W}^t_1\mathbf{q} + \mathbf{b}^t_1\right) + \mathbf{b}^t_2$ are 2-layer perceptrons with the ReLU activation function; $\mathbf{W}$ are matrices, $\mathbf{b}$ and $\mathbf{w}$ are vectors, and b is a scalar. The update functions consist of a linear transformation followed by a normalization layer, while aggregation is performed through summation. $\pi(h, q, e)$ is the score of the triple $q(h, e)$. The initialization of relations to vectors of ones, $\mathbf{1}^{d_L}$, or zeros, $\mathbf{0}^{d_L}$, and entities to $\mathbf{q}$ or zero vectors, makes the architecture of Ultra^+ generalizable to unseen relations and entities during inference. Ultra^+ uses

the binary cross entropy (BCE) loss,

$$\mathcal{L}_{\text{BCE}} = -\frac{1}{|\mathcal{T}_+|}\sum_{\tau\in\mathcal{T}_+}\Big(\log\pi(\tau) + \frac{1}{n(\tau)}\sum_{i=1}^{n(\tau)}\log\big(1-\pi(\tau_i')\big)\Big)$$

to measure the difference between predicted probabilities and triple plausibilities. The BCE loss penalizes high score for true triples, τ, low score for corrupted triples, τ_i'.

4.3 Comparing Ultra$^+$ and Motif

The KGFM Motif uses a variety of motifs (n-ary orders) to construct a relation hypergraph. The experiments in (Huang et al., 2025) are conducted on 2-path, 3-path, and k-star motifs, denoted by $\mathcal{F}_k^{path}$ and $\mathcal{F}_k^{star}$, respectively. It can be observed that Motif is unable to discriminate between closed and open paths, unlike Ultra$^+$. The second significant distinction derived from the orders. To explain this, let us consider the motifs arising from their respective 3-path based structural vocabulary. The 3-aries in Motif are named and are equivalent to ours as follows: $\text{tfh} \sim \text{fff}$, $\text{tft} \sim \text{ffr}$, $\text{hfh} \sim \text{frf}$ and $\text{hft} \sim \text{rff}$. As the IKG in Figure 3a is a directed acyclic graph, the u_v are equivalent to $\text{u}\_\text{v}_\text{o}$. Figure 3b is therefore built using the latter. From Figure 3a, r_1, r_2 and r_3 are linked by the motif tfh and $(a, r_1, b, r_2, c, r_3, d)$ is the only element in the equivalence class $\text{tfh}(r_1, r_2, r_3)$. Similarly $\text{tfh}(r_1, r_4, r_3)$ and $\text{tfh}(r_1, r_5, r_3)$ are singletons. However, the equivalence class $\text{fff}_\text{o}(r_1, r_3)$ is the union of $\text{tfh}(r_1, r_i, r_3), i = 2, 4, 5$, this is to say $\omega\left(\text{fff}_\text{o}\left(r_1, r_2, r_3\right)\right) = \sum_i \omega\left(\text{tfh}\left(r_1, r_i, r_3\right)\right)$. In general, the weights of the equivalence classes induced by Ultra$^+$'s 3-path motifs are higher than the Motif's ones.

Theorem 4.3. *Let ρ be a monomorphism from $\mathcal{P}_3$ to a graph K. If $\text{uvw}_\text{o} \circ \rho$ is an ϵ-edge and its corresponding motif in* Motif*'s vocabulary is an ϵ'-edge, then $\epsilon' \leq \epsilon$.*

Theorem 4.3 states that if no edge exists between two relations in the Ultra$^+$ relation graph, then they are not connected by a hyper-edge in the Motif relation hypergraph. This proves the robustness of Ultra$^+$. Furthermore, the theorem demonstrates that Ultra$^+$ is computationally less demanding than Motif. This difference in computation appears in the GNN$_\mathcal{G}$'s message function. In order to clarify this statement, let us consider the neighborhoods of r_3 in both relation graphs. Ultra$^+$ returns $\mathcal{N}(\text{fff}_\text{o}, r_3) = \{r_1\}$ while Motif returns $\mathcal{N}^1(\text{tfh}, r_3) = \emptyset$, $\mathcal{N}^2(\text{tfh}, r_3) = \emptyset$ and $\mathcal{N}^3(\text{tfh}, r_3) = \{r_1, r_2, r_4, r_5\}$; where the upper script ^{i} means r_3 appears at the i'th position in the hyperedge tfh. In comparison to $\mathcal{N}(\text{fff}_\text{o}, r_3)$, operations over $\mathcal{N}^3(\text{tfh}, r_3)$ result in an increase in compute time. The choice of relation embedding GNN also contributes to the increases of computing time. The HCNets used by Motif genuinely involves more computation, as it employs a learnable query vector and a sinusoidal positional encoding for each query relation q.

5 Experiments and Results

In our experiments, we aim to answer the following research questions:

(RQ1) Can the scaling behavior of recent GNN based graph foundation models be improved with the proposed extension?
(RQ2) Does the zero shot performance increase with increasing vocabulary?
(RQ3) Can the addition of specific topological graphlets (e.g., N-M graphlets) help link prediction for containing N-M relations?
(RQ4) Does enriching vocabulary with closed paths improve model performance?
(RQ5) Does constructing a relation graph with binary meta-relations offer advantages over using ternary meta-relations?

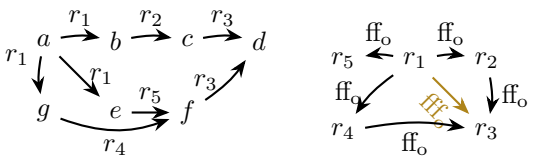

(a) Illustrative Toy KG (IKG)

(b) Relation graph of the IKG

Figure 3: (a) A toy Knowledge Graph (IKG) with five relations and seven entities, illustrating the underlying relational structure. (b) The corresponding relation graph constructed from the structural vocabulary of open paths $\{\text{ff}_\text{o}, \text{fff}_\text{o}\}$, where relations are nodes and edges capture their co-occurrence within paths.

Benchmarks and Pattern-Matched Relation Graphs. In our experiments, we assess the essence of Ultra$^+$ using 57 KGs with various characteristics. We grouped these KGs according to entity

learning (18 KGS), graph transfer (23 KGs), and transductive learning (16 KGs) tasks. Additional information about the KGs in each group is included in Appendix B. Ultra^+ is pretrained on the CoDEx Medium, FB15k237, and WN18RR KGs, and subsequently assessed in the ZSLP tasks.

Galkin et al. (2023) and Huang et al. (2025) employ sparse matrix multiplication of the (multi-relational) adjacency matrix $\mathbb{A} \in \mathbb{R}^{n\times m\times n}$ and matrices representing head-relation pair $\mathbb{E}_h \in \mathbb{R}^{n\times m}$ and tail-relation pair $\mathbb{E}_t \in \mathbb{R}^{n\times m}$. Multiplying $\mathbb{E}_{\text{x}}^T$ by $\mathbb{E}_{\text{y}}$ results into the adjacency matrix of the x2y meta-relations used in Ultra. This method provides additional information on the number of occurrences of the respective graphlet in the whole dataset. However, this information is left unused, as only the connection information is represented in the relation KG in Ultra and the relation hypergraph in Motif, respectively. As we also distinguish between closed and open path, computation via the adjacency matrix becomes computationally expensive. Pattern matching, on the other hand, can be used in a highly parallel fashion to compute the relation graph of any KG. To obtain the relation graph we construct a SPARQL ask query for each element in the vocabulary (see Appendix E.4 for the exact Queries), which can be run on any rdf KG. This method enables the computation of relation graphs based on vocabularies containing arbitrary graphlets.

Evaluation Protocol. We follow the best practices for evaluating KGE models by considering the Mean Reciprocal Rank (MRR), and the Hits at n (Hn, n = 1,3,10) metrics. Link prediction consists of finding the missing entity ? in the queries $Q = r(h, ?)$ or $Q' = r(?, t)$. First, we created a symbolic inverse relation r', which turns queries with a missing head into $Q = r'(t, ?)$. This means that we only look at queries that are in the form of Q. Next, Ultra^+ scores and ranks the corrupted triples in a decreasing order. The predicted missing entity is the top ranked corrupted entity. We compare our models against the state-of-the-art KGFMs Ultra and Motif using the aforementioned evaluation metrics. We consider six different vocabularies to design our models; namely, $\mathcal{U}_2$, $\mathcal{V}_j^- = \mathcal{V}_j \setminus \{\text{u}_\smile \text{v}_\text{c}\}$, $\mathcal{V}_j$, $\mathcal{V}_j^+ = \mathcal{V}_j \cup \mathcal{M}'_4, j = 2, 3$. We denote the Ultra^+ variant built on the vocabulary $\mathcal{X}_\bullet^\pm$ by $\text{Ultra}^+[\mathcal{X}_\bullet^\pm]$.

Results. The experimental results of evaluating the pretrained Ultra^+ on the benchmark KGs are reported in Table 1. In the following, the operator $\geq$ relating two models means that the first model *outperforms* the second model.

Table 1: Average zero-shot link prediction MRR and H10 over 51 KGs. Baseline results are taken from (Huang et al., 2025). $\mathcal{P}_n$, O and C stand for n-, open, and closed paths; and N-M stands for many-to-many subgraphs

Model	Structural Vocabulary			Ind.(e) (18 KGs)		Ind.(e, r) (23 KGs)		Transd. (10 KGs)		Total Avg. (51 KGs)	
	$\mathcal{V}$	Definition	$\#\mathcal{V}$	MRR	H10	MRR	H10	MRR	H10	MRR	H10
Ultra^+	$\mathcal{V}_2^-$	O. $\mathcal{P}_2$	4	.388	.551	.323	.498	.338	.498	.349	.516
	$\mathcal{U}_2$	$\mathcal{P}_2$	4	.425	.567	.350	.515	.343	.499	.375	.530
	$\mathcal{V}_2$	O. & C. $\mathcal{P}_2$	8	.441	.579	.354	.533	.349	.509	.384	.544
	$\mathcal{V}_2^+$	O. & C. $\mathcal{P}_2$ & N-M	16	.415	**.582**	.349	.525	.347	.504	.372	.541
	$\mathcal{V}_3^-$	O. $\mathcal{P}_3$	16	.423	.561	.337	.510	.346	.496	.369	.525
	$\mathcal{V}_3$	O. & C. $\mathcal{P}_3$	24	**.445**	.581	.355	**.542**	**.355**	**.511**	**.387**	**.549**
	$\mathcal{V}_3^+$	O. & C. $\mathcal{P}_3$ & N-M	32	.435	.581	**.356**	.532	.345	.499	.382	.543
Ultra	$\mathcal{U}_2$	$\mathcal{P}_2$	4	.431	.566	.345	.513	.339	.494	.374	.529
Motif	$\mathcal{U}_3$	$\mathcal{P}_3$	12	.436	.577	.349	.525	.343	.496	.378	.537

General Overview: Figure 4 reports the average performance of Ultra and Ultra^+ as the number of pretraining KGs increases. (**RQ1**) Ultra^+'s variants consistently outperform Ultra, demonstrating both scalability and performance gains. While $\text{Ultra}^+[\mathcal{V}_2]$ improves monotonically before saturating, $\text{Ultra}^+[\mathcal{V}_3]$ fluctuates with the addition of WN18RR and ConceptNet100k at position 2 and 6 respectively (see Table 16 for more details), highlighting the need for careful selection and ordering of pretraining KGs given their structural heterogeneity. Observing the path- and topology- based vocabulary variants, we notice that $\text{Ultra}^+[\mathcal{V}_3] \geq \text{Ultra}^+[\mathcal{V}_2] \geq \text{Ultra}^+[\mathcal{U}_2] \geq \text{Ultra}^+[\mathcal{V}_2^-]$ on average for relation learning, graph transfer, and transductive inference tasks. This trend in performance can be related to the inclusion of the vocabularies $\mathcal{V}_2^- \subset \mathcal{U}_2 \subset \mathcal{V}_2 \subset \mathcal{V}_3$. However, we have found

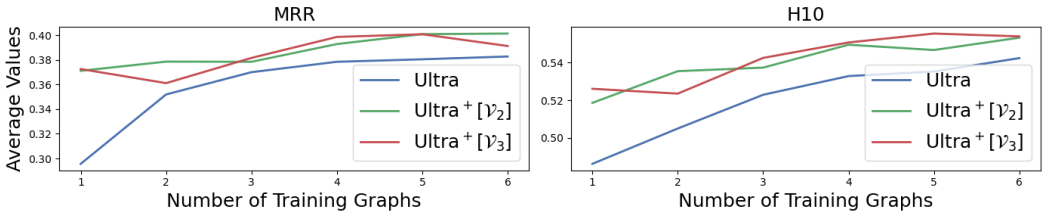

Figure 4: Average Performance over 51 Graphs of Ultra and Ultra$^+$ models pretrained on an increasing number of Graphs.

that combining the path-based and topology-based vocabularies does not result in an increase in performance as Ultra$^+[\mathcal{V}_3]$ and Ultra$^+[\mathcal{V}_2]$ often surpass Ultra$^+[\mathcal{V}_3^+]$ and Ultra$^+[\mathcal{V}_2^+]$ respectively. **(RQ2)** On one hand, we can conclude that the zero-shot performance increases with increasing the path-based vocabulary. **(RQ3)** On the other hand, mixing the topology-based with the path-based vocabulary does not necessarily preserve the performance increase.

The Motif model maintains its superiority over Ultra for all tasks. This difference in performance is a consequence of adding 3-path graphlets to Ultra's vocabulary. Although Ultra$^+[\mathcal{V}_2]$ utilized only the 2-path based vocabulary $\mathcal{V}_2$, it notably outperforms Motif and Ultra on both inductive and transductive link prediction. **(RQ4)** This clearly demonstrates the importance of having a vocabulary rich enough to convey information about closed and open paths. Ultra$^+[\mathcal{V}_3]$ is the best performing variant of the Ultra$^+$ models across all the settings. It uses the same vocabulary as Motif, except that its graphlets are positional binary orders. **(RQ5)** Thus, its superiority over Motif lies in the arity of the graphlets.

On the robustness of Ultra$^+$***:*** In all three models: Ultra$^+$, Ultra, and Motif, two relations are connected in the relation graph as soon as they co-occur at least once in the KG. For Ultra$^+$, this corresponds to observing a single match of the associated SPARQL query pattern in the KG; for Ultra and Motif, it corresponds to the relevant entry of the adjacency matrix (obtained via sparse matrix multiplication) becoming non-zero. In either case, the frequency of co-occurrence does not influence whether an edge is created. However, because Ultra$^+$ employs positional binary orders, this insensitivity to frequency is implicitly mitigated in its relation graph, as formalized in Theorem 4.3. Empirically, sparse KGs provide a natural setting for assessing the robustness of KGFMs that construct relation graphs. In our experiments, WDsinger, NELL23k, and FB15k237(10/20/50) constitute such sparse knowledge graphs.

Table 2: Comparing Ultra, Motif and Ultra$^+$ on 5 transductive sparse datasets. Baseline results are taken from (Huang et al., 2025).

Model	Ultra		Motif		Ultra$^+[\mathcal{V}_2]$		Ultra$^+[\mathcal{V}_3]$	
Dataset	**MRR**	**H10**	**MRR**	**H10**	**MRR**	**H10**	**MRR**	**H10**
WDsinger	.382	.498	.397	**.514**	**.402**	.505	**.402**	.511
NELL23k	.239	.408	.220	.384	.249	.413	**.250**	**.419**
FB15k237(10)	.248	.398	.236	.384	**.249**	**.404**	.245	.400
FB15k237(20)	.272	.436	.259	.422	**.274**	**.439**	.268	.431
FB15k237(50)	.324	.526	.312	.508	**.329**	**.527**	.326	.524

6 Conclusion

We proposed a KGFM framework called Ultra$^+$ capable of constructing a relation graph from any structural vocabulary composed of a set of graphlets. This framework enables the conversion of n-ary graphlets' orders into positional binary orders, thereby maintaining pairwise relational semantics and mitigating the complexity associated with hypergraphs. Using SPARQL to run ASK queries simplifies the distinction between open and closed paths when mining graphlets, and overcomes the major limitation of computing relation graphs when higher-order graphlets involve the full adjacency matrix. Our theoretical findings, described in Theorems 3.2 and 4.3, demonstrate that Ultra$^+$

exhibits greater robustness compared to the current baseline KGFMs. Evaluation of ZSLP tasks, with Ultra^{+} pretrained on three KGs, indicated that an increase in structural vocabulary is advantageous when only path-based vocabulary is utilized, yet it becomes detrimental when combining path- and topology-based vocabularies. We showed that enhancing the model's awareness of relational patterns and topological patterns significantly improves the model's MRR and H10, respectively.

Our Model $\mathrm{Ultra}^{+}[\mathcal{V}_3]$ achieves state-of-the-art performance in ZSLP averaged across 51 datasets with only 3 Graphs used for pretraining. Our investigation also shows that scaling pretraining has the chance to further improve performance. The case for scaling the vocabulary, on the other hand, remains ambiguous. We observed an increase in performance for increasing path based vocabulary, while adding structurally inspired graphlets seems to be detrimental. A large scale investigation of larger structural vocabularies remains challenging, due to the computational complexity of Relation Graph computation for vocabularies containing complex graphlets. We will address efficient computation of Relation Graphs that go beyond instance based computation (where existence of a single instance of a grpahlet results in a connection in the Relation Graph) in future research.

Reproducibility Statement

We publish our full implementation in an open repository: ultra-augmentations[1]. It contains model architectures, training scripts, hyperparameter configurations, dataset preprocessing code, and random seeds as well as trained checkpoints. Detailed instructions for reproducing all experiments are included to guarantee full reproducibility of our results.

References

Rishi Bommasani. On the opportunities and risks of foundation models. *arXiv preprint arXiv:2108.07258*, 2021.

Antoine Bordes, Nicolas Usunier, Alberto Garcia-Duran, Jason Weston, and Oksana Yakhnenko. Translating embeddings for modeling multi-relational data. *Advances in neural information processing systems*, 26, 2013.

Tom Brown, Benjamin Mann, Nick Ryder, Melanie Subbiah, Jared D Kaplan, Prafulla Dhariwal, Arvind Neelakantan, Pranav Shyam, Girish Sastry, Amanda Askell, et al. Language models are few-shot learners. *Advances in neural information processing systems*, 33:1877–1901, 2020.

Ling Cai, Bo Yan, Gengchen Mai, Krzysztof Janowicz, and Rui Zhu. Transgcn: Coupling transformation assumptions with graph convolutional networks for link prediction. In *Proceedings of the 10th international conference on knowledge capture*, pp. 131–138, 2019.

Yupeng Chang, Xu Wang, Jindong Wang, Yuan Wu, Linyi Yang, Kaijie Zhu, Hao Chen, Xiaoyuan Yi, Cunxiang Wang, Yidong Wang, et al. A survey on evaluation of large language models. *ACM transactions on intelligent systems and technology*, 15(3):1–45, 2024.

Lisa Ehrlinger and Wolfram Wöß. Towards a definition of knowledge graphs. *SEMANTiCS (Posters, Demos, SuCCESS)*, 48(1-4):2, 2016.

Mikhail Galkin, Xinyu Yuan, Hesham Mostafa, Jian Tang, and Zhaocheng Zhu. Towards foundation models for knowledge graph reasoning. *arXiv preprint arXiv:2310.04562*, 2023.

Mikhail Galkin, Jincheng Zhou, Bruno F Ribeiro, Jian Tang, and Zhaocheng Zhu. Zero-shot logical query reasoning on any knowledge graph. *CoRR*, 2024. URL `https://github.com/`.

Takuo Hamaguchi, Hidekazu Oiwa, Masashi Shimbo, and Yuji Matsumoto. Knowledge transfer for out-of-knowledge-base entities: A graph neural network approach. *arXiv preprint arXiv:1706.05674*, 2017.

Aidan Hogan, Eva Blomqvist, Michael Cochez, Claudia d'Amato, Gerard De Melo, Claudio Gutierrez, Sabrina Kirrane, José Emilio Labra Gayo, Roberto Navigli, Sebastian Neumaier, et al. Knowledge graphs. *ACM Computing Surveys (Csur)*, 54(4):1–37, 2021.

[1] `https://anonymous.4open.science/r/ultra-augmentations`

Xingyue Huang, Pablo Barceló, Michael M Bronstein, İsmail İlkan Ceylan, Mikhail Galkin, Juan L Reutter, and Miguel Romero Orth. How expressive are knowledge graph foundation models? *arXiv preprint arXiv:2502.13339*, 2025.

Daniel Krech, Gunnar Aastrand Grimnes, Graham Higgins, Nicholas Car, Jörn Hees, Iwan Aucamp, Niklas Lindström, Natanael Arndt, Ashley Sommer, Edmond Chuc, Ivan Herman, Alex Nelson, Jamie McCusker, Tom Gillespie, Thomas Kluyver, Florian Ludwig, Pierre-Antoine Champin, Mark Watts, Urs Holzer, Ed Summers, Whit Morriss, Donny Winston, Drew Perttula, Filip Kovacevic, Remi Chateauneu, Harold Solbrig, Benjamin Cogrel, and Veyndan Stuart. RDFLib, October 2025. URL `https://github.com/RDFLib/rdflib`.

Xi Victoria Lin, Todor Mihaylov, Mikel Artetxe, Tianlu Wang, Shuohui Chen, Daniel Simig, Myle Ott, Naman Goyal, Shruti Bhosale, Jingfei Du, et al. Few-shot learning with multilingual language models. *arXiv preprint arXiv:2112.10668*, 2021.

Yankai Lin, Zhiyuan Liu, Maosong Sun, Yang Liu, and Xuan Zhu. Learning entity and relation embeddings for knowledge graph completion. In *Twenty-ninth AAAI conference on artificial intelligence*, 2015.

Jiawei Liu, Cheng Yang, Yuan Fang, Philip S Yu, Zhiyuan Lu, Junze Chen, Yibo Li, Mengmei Zhang, Ting Bai, Lichao Sun, and Chuan Shi. Towards Graph Foundation Models: A Survey and Beyond. *35.nnnnnnn*, 1(1), 2023. doi: 10.1145/nnnnnnn.nnnnnnn.

Shuwen Liu, Bernardo Grau, Ian Horrocks, and Egor Kostylev. Indigo: Gnn-based inductive knowledge graph completion using pair-wise encoding. *Advances in Neural Information Processing Systems*, 34:2034–2045, 2021.

Haitao Mao, Zhikai Chen, Wenzhuo Tang, Jianan Zhao, Yao Ma, Tong Zhao, Neil Shah, Mikhail Galkin, and Jiliang Tang. Position: Graph Foundation Models are Already Here. 2 2024. URL `https://arxiv.org/abs/2402.02216v3`.

Ron Milo, Shai Shen-Orr, Shalev Itzkovitz, Nadav Kashtan, Dmitri Chklovskii, and Uri Alon. Network motifs: simple building blocks of complex networks. *Science*, 298(5594):824–827, 2002.

Natasha Noy, Yuqing Gao, Anshu Jain, Anant Narayanan, Alan Patterson, and Jamie Taylor. Industry-scale knowledge graphs: Lessons and challenges: Five diverse technology companies show how it's done. *Queue*, 17(2):48–75, 2019.

Shirui Pan, Linhao Luo, Yufei Wang, Chen Chen, Jiapu Wang, and Xindong Wu. Unifying large language models and knowledge graphs: A roadmap. *IEEE Transactions on Knowledge and Data Engineering*, 36(7):3580–3599, 2024.

Thomas Pellissier Tanon. Oxigraph. URL `https://github.com/oxigraph/oxigraph`.

Jorge Pérez, Marcelo Arenas, and Claudio Gutierrez. Semantics and complexity of sparql. In *International semantic web conference*, pp. 30–43. Springer, 2006.

Nataša Pržulj. Biological network comparison using graphlet degree distribution. *Bioinformatics*, 23 (2):e177–e183, 2007.

Pedro Ribeiro, Pedro Paredes, Miguel EP Silva, David Aparicio, and Fernando Silva. A survey on subgraph counting: concepts, algorithms, and applications to network motifs and graphlets. *ACM computing surveys (csur)*, 54(2):1–36, 2021.

Michael Schlichtkrull, Thomas N Kipf, Peter Bloem, Rianne Van Den Berg, Ivan Titov, and Max Welling. Modeling relational data with graph convolutional networks. In *The semantic web: 15th international conference, ESWC 2018, Heraklion, Crete, Greece, June 3–7, 2018, proceedings 15*, pp. 593–607. Springer, 2018.

Zhiqing Sun, Zhi-Hong Deng, Jian-Yun Nie, and Jian Tang. Rotate: Knowledge graph embedding by relational rotation in complex space. *arXiv preprint arXiv:1902.10197*, 2019.

Komal Teru, Etienne Denis, and Will Hamilton. Inductive relation prediction by subgraph reasoning. In *International conference on machine learning*, pp. 9448–9457. PMLR, 2020.

Quan Wang, Zhendong Mao, Bin Wang, and Li Guo. Knowledge graph embedding: A survey of approaches and applications. *IEEE transactions on knowledge and data engineering*, 29(12): 2724–2743, 2017.

Thomas Wang, Adam Roberts, Daniel Hesslow, Teven Le Scao, Hyung Won Chung, Iz Beltagy, Julien Launay, and Colin Raffel. What language model architecture and pretraining objective works best for zero-shot generalization? In *International Conference on Machine Learning*, pp. 22964–22984. PMLR, 2022.

Zehong Wang, Zheyuan Liu, Tianyi Ma, Jiazheng Li, Zheyuan Zhang, Xingbo Fu, Yiyang Li, Zhengqing Yuan, Wei Song, Yijun Ma, et al. Graph foundation models: A comprehensive survey. *arXiv preprint arXiv:2505.15116*, 2025.

Zhen Wang, Jianwen Zhang, Jianlin Feng, and Zheng Chen. Knowledge graph embedding by translating on hyperplanes. In *Proceedings of the AAAI Conference on Artificial Intelligence*, volume 28, 2014.

Jason Wei, Yi Tay, Rishi Bommasani, Colin Raffel, Barret Zoph, Sebastian Borgeaud, Dani Yogatama, Maarten Bosma, Denny Zhou, Donald Metzler, et al. Emergent abilities of large language models. *arXiv preprint arXiv:2206.07682*, 2022.

Jun Xia, Chengshuai Zhao, Bozhen Hu, Zhangyang Gao, Cheng Tan, Yue Liu, Siyuan Li, and Stan Z. Li. Mole-BERT: Rethinking pre-training graph neural networks for molecules. In *The Eleventh International Conference on Learning Representations*, 2023. URL https://openreview.net/forum?id=jevY-DtiZTR.

Lianghao Xia and Chao Huang. Anygraph: Graph foundation model in the wild, 2024. URL https://arxiv.org/abs/2408.10700.

Adnan Zeb, Summaya Saif, Junde Chen, Anwar Ul Haq, Zhiguo Gong, and Defu Zhang. Complex graph convolutional network for link prediction in knowledge graphs. *Expert Systems with Applications*, 200:116796, 2022. ISSN 0957-4174. doi: https://doi.org/10.1016/j.eswa.2022.116796. URL https://www.sciencedirect.com/science/article/pii/S0957417422002548.

Yucheng Zhang, Beatrice Bevilacqua, Mikhail Galkin, and Bruno Ribeiro. TRIX: A More Expressive Model for Zero-shot Domain Transfer in Knowledge Graphs. 2 2025. URL https://arxiv.org/pdf/2502.19512.

Wayne Xin Zhao, Kun Zhou, Junyi Li, Tianyi Tang, Xiaolei Wang, Yupeng Hou, Yingqian Min, Beichen Zhang, Junjie Zhang, Zican Dong, et al. A survey of large language models.

A Proof of the Theorems

In this section, we provide the proofs for the theorems stated in the paper. Before we begin, let us summarize the key mathematical symbols and their meanings used throughout the paper in Table 3

A.1 Proof of Theorem 3.2

Any positional m-ary order, $m < n$, spans a group of n-ary orders.

Proof. Consider two positive integers, m and n, where $m < n$. Let $\mathrm{g} = \mathrm{g}_{i_1,\ldots,i_m \leq n}$ represents a positional m-ary. According to Definition 3.1, g is a function with n arguments, out of which $n - m$ are dummy arguments. Define $\pi(i_k)$ as the position of i_k within the ordered list of all n arguments. We now consider the family of n-ary $\mathrm{g}^{(j)} = \mathrm{g}_{j_1,\ldots,j_n}$ such that if $\pi(j_l) = \pi(i_k)$, then $j_l = i_k$ for $k = 1, \ldots, m$ and $l = 1, \ldots, n$. Consequently, g is induced by any of the n-ary $\mathrm{g}^{(j)}$. In other words, the m-ary spans the aforementioned family of n-aries. □

Table 3: Notation Table.

Symbol	Meaning
$\mathcal{E}, \mathcal{R}$	Entity and relation sets
$\mathcal{T}_{,+,-}$	Set of all plausible, true ($_+$), and corrupted ($_-$) triples
$K = (\mathcal{E}^K, \mathcal{R}^K, \mathcal{T}_+^K)$	Knowledge Graph
ϕ, ρ, η	KG, relation, and entity homomorphism
$\phi_{\mathrm{g}} = (\rho, \eta) : G \xrightarrow{mon} K$	KG monomorphism with $\rho : \mathcal{R} \to \mathcal{R}^K, \eta : \mathcal{E} \to \mathcal{E}^K$ two injective maps
$card(\mathcal{G}) = \lvert\mathcal{T}\rvert$	Cardinality of the graphlet $\mathcal{G}$
$\mathcal{G}, G, \mathrm{g}$	Graphlet, small KG, and order on $\mathcal{R}$
$\mathrm{g}(\mathcal{R})$	A tuple defined by the order g on $\mathcal{R}$
$\mathrm{g}_{i_1,\ldots,i_{m\leq n}}$	(if $m < n$) positional m-, (else) n-ary order
$\mathrm{g}(\mathcal{R}^K) = \left\{\mathrm{g} \circ \rho(\mathcal{R}) \lvert \rho : \mathcal{R} \xrightarrow{mon} \mathcal{R}^K\right\}$	Ordered n-aries (of relations in $\mathcal{R}^K$) induced by g
$\phi_{\mathrm{g}}(G), \mathcal{G}(K)$	Occurrence, set of occurrences of $\mathcal{G}$ in K
$\overline{\mathrm{X}} = \{\phi'(G) \lvert \phi'(X) \equiv_{\mathrm{g}} \phi(X)\}$	Equivalence class
$(\mathcal{V}, \omega)$	Structural vocabulary, $\mathcal{V} = (\mathcal{G}_i, \mathrm{g}_i)$ a set of graphlets, $\omega(\overline{\phi(G_i)})$ a weighting function
$\mathrm{f}, \mathrm{r}, \ _{\mathrm{o}}, \_\mathrm{c}$	Forward, backward/reversed, open, and closed path
$\smile \in \{\mathrm{f}, \mathrm{r}\}^i$	A sequence of length i over the alphabets f, r.
$u \smile v = \mathrm{g}_{1,n}$	A Positional 2-ary defined by the first and last position
$\mathcal{P}_p$	Set of paths of length p
O., C., O. & C. $\mathcal{P}_p$	Open, closed, and open or closed paths of length p.
$\mathcal{V}_p = \left\{\mathrm{u}\smile\mathrm{v}_\mathrm{z} \lvert \mathrm{u}, \mathrm{v} \in \{\mathrm{f}, \mathrm{r}\}, \mathrm{z} \in \{\mathrm{o}, \mathrm{c}\}\right\}$	(O., C.) $\mathcal{P}_p$-based vocabulary
$\mathcal{U}_p = \left\{\mathrm{u}\smile\mathrm{v} \lvert \mathrm{u}, \mathrm{v} \in \{\mathrm{f}, \mathrm{r}\}, \right\}$	$\mathcal{P}_p$-based vocabulary
N-M	Many to many
$\mathcal{M}_{ij} = \{\mathrm{uv}_{i:j} \mid \mathrm{u}, \mathrm{v} \in \{\mathrm{f}, \mathrm{r}\}\}$	N-M subgraphs with i, j number of u and v edges resp.
$\mathcal{M}_m = \{\mathcal{M}_{i,j} \mid i + j = m\}$	m-star
$\mathcal{V}_p^-$	O. $\mathcal{P}_p$-based vocabulary
$\mathcal{V}_p^+$	O. & C. $\mathcal{P}_p$- and $\mathcal{M}_4$-based vocabulary
$\mathcal{N}^i(\mathrm{g}, r)$	Neighborhood of r (the ith node) relative to the n-ary g
$\mathrm{Ultra}^+[\mathcal{X}_p^\pm]$	Ultra^+ variant built on the vocabulary $\mathcal{X}_p^\pm$

A.2 Proof of Theorem 4.3

Let ρ be a monomorphism from $\mathcal{P}_3$ to a graph K. If $\mathrm{uvw_o} \circ \rho$ is an ϵ-edge and its corresponding motif in Motif's vocabulary is an ϵ'-edge, then $\epsilon' \leq \epsilon$.

Proof. Let ρ be a monomorphism from $\mathcal{P}_3$ to a graph K. $\mathrm{uvw_o}$ is a positional binary order whose second argument is the dummy argument; i.e. $\mathrm{uvw_o} = \mathrm{g}_{1,3}$. It follows from Theorem 3.2 that $\mathrm{uvw_o}$ spans a group of 3-ary, $\mathrm{g}^{(j)}$, including it corresponding motif μ. All triples in the equivalence classes $\mathrm{g}^{(j)} \circ \rho(\mathcal{R})$ are also in $\mathrm{uvw_o} \circ \rho(\mathcal{R})$, so that $\epsilon = \omega\left(\mathrm{uvw_o} \circ \rho(\mathcal{R})\right) = \sum_j \omega\left(\mathrm{g}^{(j)} \circ \rho(\mathcal{R})\right) \geq \mu \circ \rho(\mathcal{R}) = \epsilon'$ □

A.3 Expressiveness Limitation of Motif Augmented with a Closed Path Compare to Ultra^+

One of Ultra^+'s contributions is distinguishing between closed and open paths. Although the GNN architectures of Ultra^+ and Motif are different, we are interested in finding out whether Motif augmented with closed paths is more expressive than Ultra^+. Let us assume that Motif is more expressive than Ultra^+. We will now consider the cyclic KG in Figure 5 and its relation graph in the Ultra^+ and Motif framework. As this graph is symmetric, the results are independent of the choice of query relation. Let r_1 be the query relation.

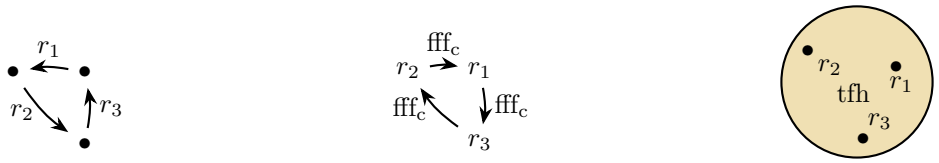

(a) Cyclic KG (b) Relation (Binary)graph (c) Relation Hypergraph

Figure 5: Cyclic Knowledge Graph and Relation Graphs: (a) A cyclic knowledge graph with three relations. (b) Ultra$^+$ constructs a relation graph consisting of three 2-ary edges, while (c) Motif constructs a relation hypergraph with a single 3-ary edge.

Relation Encoding with Motif. The relation graph, G_M, constructed in Motif framework has three edges, mainly: $\text{tfh}(r_1, r_2, r_3)$, $\text{tfh}(r_3, r_1, r_2)$, and $\text{tfh}(r_2, r_3, r_1)$. We have $\mathbf{h}^{(0)}_{r_1|r_1} = \mathbf{1}$ and $\mathbf{h}^{(0)}_{r_i|r_1} = \mathbf{0}, i \neq 1$. Thus,

$$\begin{aligned}
\mathbf{h}^{(1)}_{r_1|r_1} &= \text{UP}\big(\mathbf{h}^{(0)}_{r_1|r_1}, \text{AGG}\big[\{\text{MSG}\big(\{\big(\mathbf{h}^{(0)}_{r'|r_1}, \mathbf{tfh}\big)|r' \in \{r_2, r_3\}\}\big)\}\big]\big) \\
&= \mathbf{1}; \\
\mathbf{h}^{(1)}_{r_2|r_1} &= \text{UP}\big(\mathbf{h}^{(0)}_{r_2|r_1}, \text{AGG}\big[\{\text{MSG}\big(\{\big(\mathbf{h}^{(0)}_{r'|r_1}, \mathbf{tfh}\big)|r' \in \{r_1, r_3\}\}\big)\}\big]\big) \\
&= \mathbf{1} \times \mathbf{tfh} = \mathbf{tfh}; \\
\mathbf{h}^{(1)}_{r_3|r_1} &= \text{UP}\big(\mathbf{h}^{(0)}_{r_3|r_1}, \text{AGG}\big[\{\text{MSG}\big(\{\big(\mathbf{h}^{(0)}_{r'|r_1}, \mathbf{tfh}\big)|r' \in \{r_1, r_2\}\}\big)\}\big]\big) \\
&= \mathbf{1} \times \mathbf{tfh} = \mathbf{tfh};
\end{aligned}$$

We observe that $\mathbf{h}^{(1)}_{r_2|r_1} = \mathbf{h}^{(1)}_{r_3|r_1}$ and assume that this holds for all $t \leq T$ where $T > 1$. It follows that

$$\begin{aligned}
\mathbf{h}^{(T+1)}_{r_2|r_1} &= \text{UP}\big(\mathbf{h}^{(T)}_{r_2|r_1}, \text{AGG}\big[\{\text{MSG}\big(\{\big(\mathbf{h}^{(T)}_{r'|r_1}, \mathbf{tfh}\big)|r' \in \{r_1, r_3\}\}\big)\}\big]\big) \\
&= \mathbf{h}^{(T)}_{r_2|r_1} + (\mathbf{h}^{(T)}_{r_1|r_1} + \mathbf{h}^{(T)}_{r_3|r_1}) \times \mathbf{tfh}; \\
\mathbf{h}^{(T+1)}_{r_3|r_1} &= \text{UP}\big(\mathbf{h}^{(T)}_{r_3|r_1}, \text{AGG}\big[\{\text{MSG}\big(\{\big(\mathbf{h}^{(T)}_{r'|r_1}, \mathbf{tfh}\big)|r' \in \{r_1, r_2\}\}\big)\}\big]\big) \\
&= \mathbf{h}^{(T)}_{r_3|r_1} + (\mathbf{h}^{(T)}_{r_1|r_1} + \mathbf{h}^{(T)}_{r_2|r_1}) \times \mathbf{tfh} \\
&= \mathbf{h}^{(T)}_{r_2|r_1} + (\mathbf{h}^{(T)}_{r_1|r_1} + \mathbf{h}^{(T)}_{r_3|r_1}) \times \mathbf{tfh} \\
&= \mathbf{h}^{(T+1)}_{r_2|r_1}.
\end{aligned}$$

Thus, Motif can't differentiate r_2 from r_3.

Relation Encoding with Ultra$^+$. On the other hand, from $\mathbf{h}^{(0)}_{r_1|r_1} = \mathbf{1}$ and $\mathbf{h}^{(0)}_{r_i|r_1} = \mathbf{0}, i \neq 1$, Ultra$^+$'s relation embedding yields

$$\begin{aligned}
\mathbf{h}^{(1)}_{r_1|r_1} &= \text{UP}\big(\mathbf{h}^{(0)}_{r_1|r_1}, \text{AGG}\big[\{\text{MSG}\big(\{\big(\mathbf{h}^{(0)}_{r'|r_1}, \mathbf{fff_c}\big)|r' \in \{r_2\}\}\big)\}\big]\big) \\
&= \mathbf{1}; \\
\mathbf{h}^{(1)}_{r_2|r_1} &= \text{UP}\big(\mathbf{h}^{(0)}_{r_2|r_1}, \text{AGG}\big[\{\text{MSG}\big(\{\big(\mathbf{h}^{(0)}_{r'|r_1}, \mathbf{fff_c}\big)|r' \in \{r_3\}\}\big)\}\big]\big) \\
&= \mathbf{0}; \\
\mathbf{h}^{(1)}_{r_3|r_1} &= \text{UP}\big(\mathbf{h}^{(0)}_{r_3|r_1}, \text{AGG}\big[\{\text{MSG}\big(\{\big(\mathbf{h}^{(0)}_{r'|r_1}, \mathbf{fff_c}\big)|r' \in \{r_1\}\}\big)\}\big]\big) \\
&= \mathbf{1} \times \mathbf{fff_c} = \mathbf{fff_c}.
\end{aligned}$$

Since $\mathbf{h}^{(1)}_{r_2|r_1} \neq \mathbf{h}^{(1)}_{r_3|r_1}$, let us assume that $\mathbf{h}^{(t)}_{r_{2,3}|r_1}$ are distinct vectors for $t < T$ except for $\mathbf{h}^{(T)}_{r_2|r_1} = \mathbf{h}^{(T)}_{r_3|r_1} = \mathbf{c}_T$. We would then have

$$\begin{aligned}
\mathbf{h}^{(T+1)}_{r_1|r_1} &= \mathrm{UP}\big(\mathbf{h}^{(T)}_{r_1|r_1}, \mathrm{AGG}\big[\{\mathrm{MSG}\big(\{\big(\mathbf{h}^{(T)}_{r'|r_1}, \mathbf{fff_c}\big)|r' \in \{r_2\}\}\big)\}\big]\big) \\
&= \mathbf{h}^{(T)}_{r_1|r_1} + \mathbf{c}_T \times \mathbf{fff_c}; \\
\mathbf{h}^{(T+1)}_{r_2|r_1} &= \mathrm{UP}\big(\mathbf{h}^{(T)}_{r_2|r_1}, \mathrm{AGG}\big[\{\mathrm{MSG}\big(\{\big(\mathbf{h}^{(T)}_{r'|r_1}, \mathbf{fff_c}\big)|r' \in \{r_3\}\}\big)\}\big]\big) \\
&= \mathbf{c}_T + \mathbf{c}_T \times \mathbf{fff_c}; \\
\mathbf{h}^{(T+1)}_{r_3|r_1} &= \mathrm{UP}\big(\mathbf{h}^{(T)}_{r_3|r_1}, \mathrm{AGG}\big[\{\mathrm{MSG}\big(\{\big(\mathbf{h}^{(T)}_{r'|r_1}, \mathbf{fff_c}\big)|r' \in \{r_1\}\}\big)\}\big]\big) \\
&= \mathbf{c}_T + \mathbf{h}^{(T)}_{r_1|r_1} \times \mathbf{fff_c} \\
&\neq \mathbf{h}^{(T+1)}_{r_2|r_1}
\end{aligned}$$

since $\mathbf{h}^{(t)}_{r_1|r_1}$ and $\mathbf{c}_t$ are multivalued polynomials of indeterminate $\mathbf{fff_c}$ and constant terms $\mathbf{1}$ and $\mathbf{0}$ respectively. In other words, Ultra^+ is able to distinguish between r_2 and r_3. This contradicts our assumption about the expressive power of Motif.

We can then conclude that Ultra^+ is at least as expressive as Motif.

B Datasets

Our Experiments have been performed on a multitude of datasets, following (Galkin et al., 2023). These datasets can be grouped into the following three subsets:

- **Inductive** (e, r): Inductive link prediction datasets with prediction on new nodes and new relations.
- **Inductive** (e): Datasets for inductive Link prediction on new nodes.
- **Transductive**: Transductive Link prediction on seen nodes and relations.

Datasets and corresponding statistics are displayed in tables 4-6.

C Additional Results

In tables 7 - 9 we display the zero shot results of Ultra and our models Ultra^+ on all datasets. Here we show the models that have been pre-trained on a mixture of 3 graphs (see Table 16).

Additionally we performed finetuning of our best model on all datasets considered here. The detailed results are displayed in Tables 11, 10 and 12. For finetuning we employed dataset specific hyperparameters as displayed in table 14. Hyperparameters common to all datasets are in table 15. Due to hardware constraints we used we used a lower batch size compared to (Galkin et al., 2023), (Zhang et al., 2025) and (Huang et al., 2025) which might reduce the finetuned performance for Datasets trained with partial datasets.

D Pretraining Scaling

We investigated the scaling behavior of our approach with different sizes of the relational vocabulary. For each vocabulary set detailed above we conducted pretraining on each of the pretraining mixtures employed in (Galkin et al., 2023) (see Table 16). Compared to (Galkin et al., 2023) we had to decrease the batch sizes to be able to train all models with the same parameters.

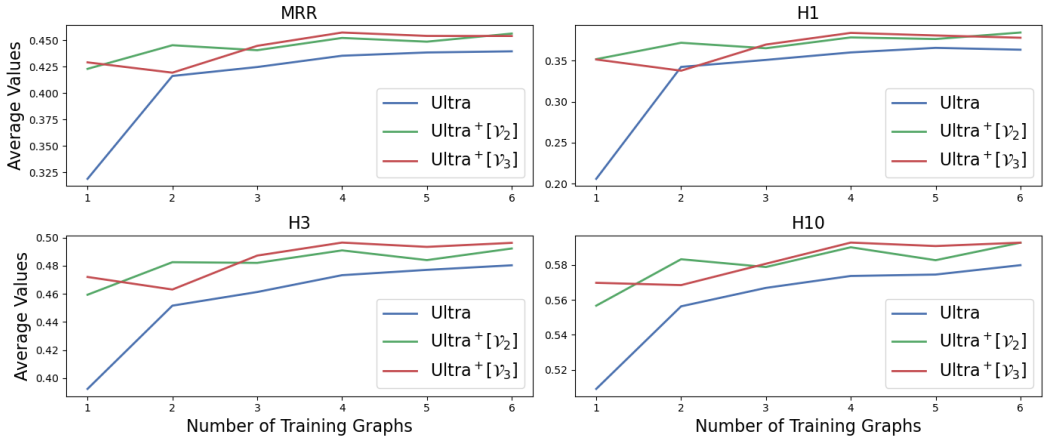

Figure 6: Average performance on 18 inductive (e) datasets of our Ultra^+ models compared with Ultra, pretrained on 1 - 6 pretraining Graphs (see Table 16).

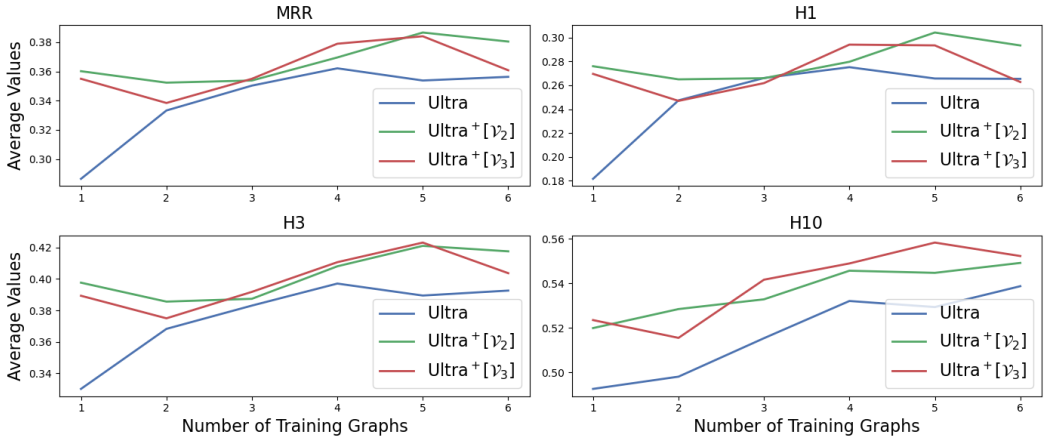

Figure 7: Average performance on 23 inductive (e,r) datasets of our Ultra^+ models compared with Ultra, pretrained on 1 - 6 pretraining Graphs (see Table 16).

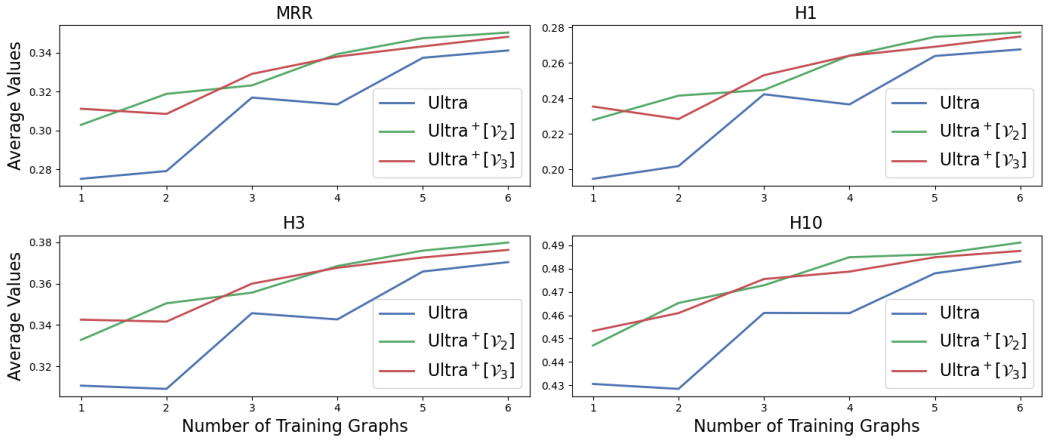

Figure 8: Average performance on 10 transductive datasets of our Ultra^+ models compared with Ultra, pretrained on 1 - 6 pretraining Graphs (see Table 16).

Table 4: Statistics of **inductive** (e, r) link prediction datasets. Triples are the number of edges given at training, validation, or test graphs, respectively, whereas Valid and Test denote triples to be predicted in the validation and test graphs.

Dataset	Training Graph			Validation Graph				Test Graph			
	Entities	Rels	Triples	Entities	Rels	Triples	Valid	Entities	Rels	Triples	Test
FB-25	5190	163	91571	4097	216	17147	5716	4097	216	17147	5716
FB-50	5190	153	85375	4445	205	11636	3879	4445	205	11636	3879
FB-75	4659	134	62809	2792	186	9316	3106	2792	186	9316	3106
FB-100	4659	134	62809	2624	77	6987	2329	2624	77	6987	2329
WK-25	12659	47	41873	3228	74	3391	1130	3228	74	3391	1131
WK-50	12022	72	82481	9328	93	9672	3224	9328	93	9672	3225
WK-75	6853	52	28741	2722	65	3430	1143	2722	65	3430	1144
WK-100	9784	67	49875	12136	37	13487	4496	12136	37	13487	4496
NL-0	1814	134	7796	2026	112	2287	763	2026	112	2287	763
NL-25	4396	106	17578	2146	120	2230	743	2146	120	2230	744
NL-50	4396	106	17578	2335	119	2576	859	2335	119	2576	859
NL-75	2607	96	11058	1578	116	1818	606	1578	116	1818	607
NL-100	1258	55	7832	1709	53	2378	793	1709	53	2378	793
Metafam	1316	28	13821	1316	28	13821	590	656	28	7257	184
FBNELL	4636	100	10275	4636	100	10275	1055	4752	183	10685	597
Wiki MT1 tax	10000	10	17178	10000	10	17178	1908	10000	9	16526	1834
Wiki MT1 health	10000	7	14371	10000	7	14371	1596	10000	7	14110	1566
Wiki MT2 org	10000	10	23233	10000	10	23233	2581	10000	11	21976	2441
Wiki MT2 sci	10000	16	16471	10000	16	16471	1830	10000	16	14852	1650
Wiki MT3 art	10000	45	27262	10000	45	27262	3026	10000	45	28023	3113
Wiki MT3 infra	10000	24	21990	10000	24	21990	2443	10000	27	21646	2405
Wiki MT4 sci	10000	42	12576	10000	42	12576	1397	10000	42	12516	1388
Wiki MT4 health	10000	21	15539	10000	21	15539	1725	10000	20	15337	1703

Table 5: Statistics of inductive (e) link prediction datasets. Triples are the number of edges given at training, validation, or test graphs, respectively, whereas Valid and Test denote triples to be predicted in the validation and test graphs.

Dataset	Rels	Training Graph		Validation Graph			Test Graph		
		Entities	Triples	Entities	Triples	Valid	Entities	Triples	Test
FB-v1	180	1594	4245	1594	4245	489	1093	1993	411
FB-v2	200	2608	9739	2608	9739	1166	1660	4145	947
FB-v3	215	3668	17986	3668	17986	2194	2501	7406	1731
FB-v4	219	4707	27203	4707	27203	3352	3051	11714	2840
WN-v1	9	2746	5410	2746	5410	630	922	1618	373
WN-v2	10	6954	15262	6954	15262	1838	2757	4011	852
WN-v3	11	12078	25901	12078	25901	3097	5084	6327	1143
WN-v4	9	3861	7940	3861	7940	934	7084	12334	2823
NL-v1	14	3103	4687	3103	4687	414	225	833	201
NL-v2	88	2564	8219	2564	8219	922	2086	4586	935
NL-v3	142	4647	16393	4647	16393	1851	3566	8048	1620
NL-v4	76	2092	7546	2092	7546	876	2795	7073	1447
ILPC Small	48	10230	78616	6653	20960	2908	6653	20960	2902
ILPC Large	65	46626	202446	29246	77044	10179	29246	77044	10184
HM 1k	11	36237	93364	36311	93364	1771	9899	18638	476
HM 3k	11	32118	71097	32250	71097	1201	19218	38285	1349
HM 5k	11	28601	57601	28744	57601	900	23792	48425	2124
HM Indigo	229	12721	121601	12797	121601	14121	14775	250195	14904

Table 6: Statistics of transductive link prediction datasets. Task denotes the prediction task: h/t is predicting both heads and tails, and t is predicting only tails.

Dataset	Entities	Rels	Train	Valid	Test	Task
FB15k237	14541	237	272115	17535	20466	h/t
WN18RR	40943	11	86835	3034	3134	h/t
CoDEx Small	2034	42	32888	1827	1828	h/t
CoDEx Medium	17050	51	185584	10310	10311	h/t
CoDEx Large	77951	69	551193	30622	30622	h/t
NELL995	74536	200	149678	543	2818	h/t
YAGO310	123182	37	1079040	5000	5000	h/t
WDsinger	10282	135	16142	2163	2203	h/t
NELL23k	22925	200	25445	4961	4952	h/t
FB15k237(10)	11512	237	27211	15624	18150	t
FB15k237(20)	13166	237	54423	16963	19776	t
FB15k237(50)	14149	237	136057	17449	20324	t
Hetionet	45158	24	2025177	112510	112510	h/t
ConceptNet100k	78334	34	100000	1200	1200	h/t

Table 7: Full results for Ultra and Ultra$^+$ models on 10 transductive datasets. Baseline results are taken from (Huang et al., 2025).

Model	Ultra		Ultra$^+$											
Vocab.	$\mathcal{U}$		$\mathcal{V}_2^-$		$\mathcal{V}_2$		$\mathcal{V}_2^+$		$\mathcal{V}_3^-$		$\mathcal{V}_3$		$\mathcal{V}_3^+$	
Dataset	**MRR**	**H10**	**MRR**	**H10**	**MRR**	**H10**	**MRR**	**H10**	**MRR**	**H10**	**MRR**	**H10**	**MRR**	**H10**
CoDExSmall	.479	.668	.469	**.675**	**.486**	.675	.480	.675	.475	.667	.484	.674	.475	.671
CoDExLarge	.339	.466	.343	.470	.342	.471	.336	.466	**.343**	**.473**	.340	.468	.335	.462
NELL995	.444	.583	.461	.598	.446	.600	**.507**	**.644**	.472	.601	.451	.613	.484	.637
YAGO310	.438	.604	.395	.570	.416	.639	.420	.607	.473	.649	**.505**	**.669**	.411	.587
WDsinger	.388	.495	.363	.500	.402	.505	.392	**.512**	.388	.503	**.402**	.511	.401	.509
NELL23k	.228	.392	.224	.392	.249	.413	.238	.405	.224	.388	**.250**	**.419**	.241	.401
FB15k237(10)	.237	.403	.245	.400	**.249**	**.404**	.244	.395	.233	.382	.245	.400	.240	.390
FB15k237(20)	.268	.436	.271	.438	**.274**	**.439**	.270	.433	.265	.425	.268	.431	.238	.398
FB15k237(50)	.323	.525	.325	.525	**.329**	**.527**	.324	.526	.323	.519	.326	.524	.313	.502
Hetionet	.287	**.417**	.282	.410	**.301**	.417	.259	.381			.278	.405	.280	.390

E Details on Relation Graph Computation

E.1 Complexity Analysis

The time complexity of Ultra and Motif are computed in (Huang et al., 2025). This involves *(i)* estimating the computational complexity of generating the relation graph, by scanning the triples in the KGs and executing the sparse-matrix multiplication, *(ii)* in addition to applying a single forward pass in both the relation and entity encoders. These are

$$\mathcal{O}\left(\left(\mid \mathcal{E} \mid^2 \mid \mathcal{R} \mid + \mid \mathcal{E} \mid\mid \mathcal{R} \mid^2\right) + L\left(\mid \mathcal{R} \mid^2 d+ \mid \mathcal{R} \mid d^2\right) + L\left(\mid \mathcal{T} \mid d+ \mid \mathcal{E} \mid d^2\right)\right) \tag{2}$$

for Ultra and Motif equipped with 2-paths, and

$$\mathcal{O}\left(\left(\mid \mathcal{E} \mid\mid \mathcal{R} \mid^3 + \mid \mathcal{E} \mid^2 \mid \mathcal{R} \mid^2\right) + L\left(\mid \mathcal{R} \mid^3 d+ \mid \mathcal{R} \mid d^2\right) + L\left(\mid \mathcal{T} \mid d+ \mid \mathcal{E} \mid d^2\right)\right) \tag{3}$$

for Motif equipped with 3-paths. Ultra$^+$ replaces step *(i)* by running SPARQL ASK queries on the KGs. This implies we only need to scan the KGs without executing the SPMMs. Since the SPARQL queries in the vocabularies we defined are bounded in size and the filter conditions are simple equalities, their time complexity is $\mathcal{O}(1)$ (refer to Theorem 1 in (Pérez et al., 2006). Thus, we reduced the time complexity for 2-paths from $\mathcal{O}\left(\mid \mathcal{E} \mid^2 \mid \mathcal{R} \mid + \mid \mathcal{E} \mid\mid \mathcal{R} \mid^2\right)$ to $\mathcal{O}\left(\mid \mathcal{E} \mid^2 \mid \mathcal{R} \mid\right)$ and for 3-paths from $\mathcal{O}\left(\mid \mathcal{E} \mid\mid \mathcal{R} \mid^3 + \mid \mathcal{E} \mid^2 \mid \mathcal{R} \mid^2\right)$ to $\mathcal{O}\left(\mid \mathcal{E} \mid\mid \mathcal{R} \mid^3\right)$. As Ultra$^+$ constructs binary relation

Table 8: Full results for Ultra and Ultra$^+$ models on 23 inductive (e, r) datasets. Baseline results are taken from (Huang et al., 2025).

Model	Ultra		Ultra$^+$											
Vocab.	$\mathcal{U}$		$\mathcal{V}_2^-$		$\mathcal{V}_2$		$\mathcal{V}_2^+$		$\mathcal{V}_3^-$		$\mathcal{V}_3$		$\mathcal{V}_3^+$	
Dataset	**MRR**	**H10**	**MRR**	**H10**	**MRR**	**H10**	**MRR**	**H10**	**MRR**	**H10**	**MRR**	**H10**	**MRR**	**H10**
FB-25	.385	.636	.386	.639	**.396**	.639	.394	**.647**	.384	.638	.393	.643	.391	.645
FB-50	.332	.535	.329	.540	.339	.548	.339	**.551**	.330	.543	.341	.546	**.343**	.547
FB-75	.397	.596	**.404**	**.609**	.404	.605	.403	.607	.399	.604	.404	.605	.398	.603
FB-100	.443	.626	.435	.627	**.443**	.625	.439	.633	.438	.628	.443	**.641**	.431	.638
WK-25	.301	.505	.284	.488	**.324**	**.530**	.280	.486	.293	.505	.304	.491	.305	.503
WK-50	.157	.305	.130	.287	**.174**	**.321**	.168	.315	.159	.285	.168	.319	.166	.307
WK-75	.375	**.538**	.373	.517	**.380**	.537	.367	.516	.364	.533	.371	.533	.374	.524
WK-100	.180	.298	.169	.294	.180	.302	.175	.294	.176	.291	.173	.291	**.185**	**.307**
NL-0	.334	.510	.318	.502	.367	.551	.336	.525	.303	.505	**.370**	**.566**	.364	.546
NL-25	.373	.544	.313	.495	.370	.552	.349	.507	.358	.542	.349	**.585**	**.391**	.573
NL-50	.389	.536	.358	.531	**.406**	**.579**	.349	.538	.364	.554	.382	.563	.393	.568
NL-75	.336	.528	.307	.487	.348	.529	.302	.495	.316	.490	.348	.539	**.349**	**.546**
NL-100	.442	.636	.401	.627	.477	.681	.449	.660	.444	.657	.479	**.694**	**.483**	.690
Metafam	.428	.739	.156	.503	.262	.723	**.484**	**.962**	.173	.560	.279	.851	.310	.872
FBNELL	.461	.631	.463	.634	.484	.659	.482	.652	.471	.640	.492	.647	**.496**	**.679**
Wiki MT1 tax	.240	.306	.150	.300	.260	**.436**	.251	.311	.234	.347	**.286**	.433	.238	.305
Wiki MT1 health	.327	.430	.291	.394	.362	.432	.312	.400	.373	.457	**.375**	**.458**	.363	.449
Wiki MT2 org	.089	.152	.096	.157	**.098**	.158	.091	.156	.096	.159	.098	**.163**	.096	.159
Wiki MT2 sci	.263	.415	.262	.387	.283	.450	.283	.424	.266	.427	**.300**	**.458**	.270	.380
Wiki MT3 art	.262	.413	.272	.420	.276	.422	.277	.429	.277	.429	**.286**	**.435**	.278	.420
Wiki MT3 infra	.634	.769	.647	**.791**	.637	.783	.640	.774	.624	.755	**.647**	.782	.638	.765
Wiki MT4 sci	.285	.449	.295	.469	.301	.464	.294	.466	**.301**	.465	.295	**.471**	.296	.463
Wiki MT4 health	**.625**	**.755**	.595	.746	.568	.729	.558	.723	.598	.729	.583	.744	.619	.746

Table 9: Full results for Ultra and Ultra$^+$ models on 18 inductive (e) datasets. Baseline results are taken from (Huang et al., 2025).

Model	Ultra		Ultra$^+$											
Vocab.	$\mathcal{U}$		$\mathcal{V}_2^-$		$\mathcal{V}_2$		$\mathcal{V}_2^+$		$\mathcal{V}_3^-$		$\mathcal{V}_3$		$\mathcal{V}_3^+$	
Dataset	**MRR**	**H10**	**MRR**	**H10**	**MRR**	**H10**	**MRR**	**H10**	**MRR**	**H10**	**MRR**	**H10**	**MRR**	**H10**
FB-v1	.498	.653	.468	.656	.498	.661	.477	.670	.492	**.687**	**.503**	.663	.503	.678
FB-v2	.504	.695	.502	.707	.510	.703	.512	.697	.507	**.718**	**.529**	.716	.525	.712
FB-v3	.489	.656	.479	.648	.488	.650	.489	.661	.488	.654	**.497**	.660	.494	**.661**
FB-v4	.478	.665	.477	.675	.488	.675	.485	.678	.474	.670	**.489**	**.679**	.489	.677
WN-v1	.658	.764	.203	.555	**.705**	.792	.697	.796	.655	.763	.703	**.811**	.690	.794
WN-v2	.648	.749	.642	.762	**.698**	.786	.455	.741	.637	.743	.676	.783	.687	**.789**
WN-v3	.367	.464	.387	.505	.361	.514	.358	.523	.373	.479	**.416**	.539	.413	**.542**
WN-v4	.603	.704	.598	.711	.651	.730	.568	.718	.605	.711	**.657**	**.738**	.644	.723
NL-v1	.694	.896	.524	.771	.739	.920	.583	.866	.597	.644	**.749**	**.930**	.585	.866
NL-v2	.516	.715	.507	.699	.551	.728	.550	.750	.528	.735	.565	.754	**.572**	**.763**
NL-v3	.510	.690	.493	.666	.550	.728	.548	.729	.526	.723	**.562**	.737	.560	**.750**
NL-v4	.483	.704	.491	.715	.505	.728	.517	.746	.505	.730	.510	.737	**.521**	**.756**
ILPC small	.296	.445	**.304**	.450	.299	.450	.295	.454	.303	.447	.301	.450	.304	**.456**
ILPC large	.292	.417	**.305**	**.427**	.287	.423	.290	.426	.299	.424	.297	.419	.297	.423
HM 1k	.058	.122	.064	.126	.065	.122	**.079**	**.147**	.079	.132	.042	.068	.036	.076
HM 3k	.055	.112	.048	.095	.046	.079	**.065**	**.116**	.056	.101	.039	.063	.034	.078
HM 5k	.051	.103	.045	.091	.043	.080	**.057**	**.104**	.051	.093	.032	.054	.030	.070
HM indigo	.446	.649	.439	.649	.446	.649	**.449**	**.654**	.432	.644	.440	.651	.438	.650

graphs, Ultra and Ultra$^+$ have the same forward pass time complexity for both 2- and 3-paths. In overall,

$$\mathcal{O}\left(\mid \mathcal{E} \mid^2 \mid \mathcal{R} \mid + L\left(\mid \mathcal{R} \mid^2 d + \mid \mathcal{R} \mid d^2\right) + L\left(\mid \mathcal{T} \mid d + \mid \mathcal{E} \mid d^2\right)\right) \tag{4}$$

Table 10: Finetuned Inductive (e, r) Performance Comparison

Dataset	Ultra		Motif		Ultra$^+[\mathcal{V}_3^+]$	
	MRR	H@10	MRR	H@10	MRR	H@10
FB-25	0.383	0.635	0.388	0.635	**0.391**	**0.642**
FB-50	0.334	0.538	**0.340**	**0.544**	0.333	0.541
FB-75	0.400	0.598	0.399	**0.607**	**0.403**	0.604
FB-100	0.444	**0.643**	0.439	0.642	**0.445**	0.640
WK-25	**0.321**	**0.535**	0.317	0.505	0.298	0.487
WK-50	0.140	0.280	0.160	0.304	**0.162**	**0.314**
WK-75	0.380	0.530	0.371	**0.535**	**0.387**	0.529
WK-100	0.168	0.286	0.173	0.284	**0.180**	**0.294**
NL-0	**0.329**	0.551	0.328	**0.556**	0.305	0.490
NL-25	**0.407**	**0.596**	0.390	0.580	0.353	0.540
NL-50	**0.418**	**0.595**	0.414	0.573	0.399	0.579
NL-75	**0.374**	**0.570**	0.360	0.548	0.360	0.563
NL-100	0.458	**0.684**	0.464	0.682	**0.477**	0.661
Metafam	0.997	**1.000**	**1.000**	**1.000**	**1.000**	**1.000**
FBNELL	**0.481**	0.661	**0.481**	**0.664**	0.445	0.626
MT1-tax	0.330	0.459	0.416	0.522	**0.429**	**0.533**
MT1-health	0.380	0.467	0.385	**0.473**	**0.386**	0.462
MT2-org	0.104	0.170	**0.106**	0.170	0.104	**0.175**
MT2-sci	0.311	0.451	**0.326**	**0.520**	0.320	0.427
MT3-art	0.306	0.473	**0.315**	0.469	**0.315**	**0.479**
MT3-infra	0.657	0.807	**0.683**	**0.827**	**0.683**	0.821
MT4-sci	0.303	0.478	0.309	0.483	**0.311**	**0.489**
MT4-health	0.704	0.785	0.703	0.787	**0.709**	**0.788**

Table 11: Finetuned Inductive (e) Performance Comparison

Dataset	Ultra		Motif		Ultra$^+[\mathcal{V}_3^+]$	
	MRR	H@10	MRR	H@10	MRR	H@10
FB-v1	0.509	0.670	**0.530**	**0.702**	0.510	0.669
FB-v2	0.524	0.710	**0.557**	**0.744**	0.540	0.730
FB-v3	0.504	0.663	**0.519**	**0.684**	0.509	0.665
FB-v4	0.496	0.684	**0.508**	**0.695**	0.497	0.683
WN-v1	0.685	0.793	0.703	**0.806**	**0.705**	0.789
WN-v2	0.679	0.779	0.680	**0.781**	**0.694**	0.779
WN-v3	0.411	0.546	**0.466**	**0.590**	0.433	0.550
WN-v4	0.614	0.720	0.659	0.733	**0.662**	**0.748**
NL-v1	0.757	0.878	0.712	0.873	**0.811**	**0.931**
NL-v2	**0.575**	0.761	0.566	**0.765**	0.572	0.761
NL-v3	0.563	0.755	0.580	0.764	**0.589**	**0.781**
NL-v4	0.469	0.733	0.507	0.740	**0.537**	**0.761**
ILPC Small	0.303	**0.453**	0.302	0.449	**0.307**	0.450
ILPC Large	**0.308**	0.431	0.307	**0.432**	0.313	**0.435**
HM-1k	0.042	0.100	**0.067**	**0.107**	0.043	0.098
HM-3k	0.030	0.090	**0.054**	**0.103**	0.025	0.062
HM-5k	0.025	0.068	**0.049**	**0.091**	0.025	0.050
HM-Indigo	**0.432**	**0.639**	0.426	0.635	0.393	0.520

Table 12: Finetuned Transductive Performance Comparison

Dataset	Ultra		Motif		Ultra$^+[\mathcal{V}_3^+]$	
	MRR	H@10	MRR	H@10	MRR	H@10
CoDEx Small	0.490	**0.686**	0.490	0.680	**0.496**	0.684
CoDEx Large	0.343	0.478	0.355	0.489	**0.359**	**0.495**
NELL-995	0.509	0.660	0.514	0.655	**0.547**	**0.678**
YAGO310	0.557	0.710	0.603	**0.735**	**0.607**	**0.735**
WDsinger	0.417	0.526	0.423	0.532	**0.431**	**0.535**
NELL23k	0.268	0.450	0.256	0.441	**0.270**	**0.453**
FB15k237(10)	0.254	0.411	0.254	0.411	**0.263**	**0.416**
FB15k237(20)	0.274	**0.445**	0.273	0.444	**0.281**	**0.445**
FB15k237(50)	0.325	0.528	0.323	0.523	**0.335**	**0.531**
Hetionet	0.399	0.538	0.446	0.575	**0.464**	**0.599**

Table 13: Average finetuned link prediction MRR and H10 over 51 KGs. Baseline results are taken from (Huang et al., 2025). $\mathcal{P}_n$, O and C stand for n-, open, and closed paths; and N-M stands for many-to-many subgraphs

Model	Structural Vocabulary			Ind.(e) (18 KGs)		Ind.(e,r) (23 KGs)		Transd. (10 KGs)		Total Avg. (51 KGs)	
	$\mathcal{V}$	Definition	$\#\mathcal{V}$	MRR	H10	MRR	H10	MRR	H10	MRR	H10
Ultra	$\mathcal{U}_2$	$\mathcal{P}_2$	4	.442	.582	.397	.556	.384	.543	.410	.563
Motif	$\mathcal{U}_3$	$\mathcal{P}_3$	12	**.455**	**.594**	**.401**	**.558**	.394	.549	.419	**.569**
Ultra$^+$	$\mathcal{V}_3$	O. & C. $\mathcal{P}_3$	24	**.455**	.581	.400	.551	**.405**	**.557**	**.420**	.563

for Ultra$^+$ equipped with 2-paths, and

$$\mathcal{O}\left(\mid \mathcal{E} \mid\mid \mathcal{R} \mid^3 + L\left(\mid \mathcal{R} \mid^2 d+ \mid \mathcal{R} \mid d^2\right) + L\left(\mid \mathcal{T} \mid d+ \mid \mathcal{E} \mid d^2\right)\right) \tag{5}$$

for Ultra$^+$ equipped with 3-paths.

E.2 Experimental Analysis

In Table 17, we compare the computation of relation graphs based on sparse matrix multiplication with query-based computation.

Implementation and Experiment Details Batching is used in the implementation of the SPMM-based computation of the relation graph, since the intermediate matrix products are too large to fit into memory. Further improvements to our implementation are possible, but not to the extent that the computation will reach the speed of Query based computations.

The Query based relation graph computation was implemented using rdflib (Krech et al., 2025) and the oxrdflib extension based on oxigraph (Pellissier Tanon) which provides efficient SPARQL query resolution and supports large datasets.

This comparison has been executed on a Machine with 64cpu (2 * 32 core AMD EPYC) cores 256GB RAM and an Nvidia A100 (80GB) GPU.

E.3 SPMM formulation of Ultra$^+$ Vocabulary

The adjacency matrices for the relation graphs in (Galkin et al., 2023) and (Huang et al., 2025) had convenient representaitons in terms of Sparse Matrix Multiplications (SPMM) expressed as products of the adjacency matrix $A \in \mathbb{R}^{n\times n}$ of the KG and two matrices $\mathbb{E}_h \in \mathbb{R}^{n\times m}$ and $E_t \in \mathbb{R}^{m\times n}$. The following formulas are used to construct the binary edges of the relation graph in Motif (see Section F in (Huang et al., 2025)) and Ultra (see Section B in (Galkin et al., 2023)):

Table 14: Hyperparameters for fine-tuning Ultra^+. Full represents a whole epoch with the entire dataset being used

Datasets	Epoch	Batch per Epoch
FB 25-100	3	full
WK 25-100	3	full
NL 0-100	3	full
MT1-MT4	3	full
Metafam, FBNELL	3	full
FB v1-v4	1	full
WN v1-v4	1	full
NL v1-v4	3	full
ILPC Small	3	full
ILPC Large	1	1000
HM 1k-5k, Indigo	1	100
FB15k237	1	full
WN18RR	1	full
CoDEx Small	1	4000
CoDEx Medium	1	4000
CoDEx Large	1	2000
NELL-995	1	full
YAGO310	1	2000
WDsinger	3	full
NELL23k	3	full
FB15k237(10)	1	full
FB15k237(20)	1	full
FB15k237(50)	1	1000
Hetionet	1	4000

Table 15: Global hyper-parameters for fine-tuning.

Hyperparameter	Value
Optimizer	AdamW
Learning rate	0.0005
Adversarial temperature	1
# Negatives	256
Batch size	8
# Repetitions	1

Table 16: Graphs and training parameters in different pre-training mixtures in Figures 6, 7 and 8

	1	2	3	4	5	6
FB15k237	✓	✓	✓	✓	✓	✓
WN18RR		✓	✓	✓	✓	✓
CoDEx-M			✓	✓	✓	✓
NELL995				✓	✓	✓
YAGO 310					✓	✓
ConceptNet100k						✓
Batch size	32	16	16	16	8	8
# steps	200,000	400,000	300,000	400,000	200,000	200,000

$$\boldsymbol{A}_{h2h} = \text{spmm}\left(\boldsymbol{E}_h^T, \boldsymbol{E}_h\right) \in \mathbb{R}^{m \times m}$$
$$\boldsymbol{A}_{t2t} = \text{spmm}\left(\boldsymbol{E}_t^T, \boldsymbol{E}_t\right) \in \mathbb{R}^{m \times m}$$
$$\boldsymbol{A}_{h2t} = \text{spmm}\left(\boldsymbol{E}_h^T, \boldsymbol{E}_t\right) \in \mathbb{R}^{m \times m}$$
$$\boldsymbol{A}_{t2h} = \text{spmm}\left(\boldsymbol{E}_t^T, \boldsymbol{E}_h\right) \in \mathbb{R}^{m \times m}$$

Table 17: Runtime and memory usage comparison for relation graph computation using $\mathcal{V}_2$ with the formulation in E.3 and the Query based computation. Time is displayed in hours:minutes:seconds

Dataset	Query based			SPMM		
	time	RAM usage	VRAM usage	time	RAM	VRAM (GPU)
WM18RR	00:00:08	10 GB	–	00:10:24	10 GB	50 GB
FB15k237	00:01:03	23 GB	–	01:52:43	40 GB	50 GB
CODEX Medium	00:00:30	12 GB	–	01:07:52	10 GB	50 GB

and the 3-ary edges in Motif:

$$\begin{aligned}
\boldsymbol{A}_{hfh} &= \operatorname{spmm}\left(\boldsymbol{E}_h^T, \boldsymbol{A}, \boldsymbol{E}_h\right) \in \mathbb{R}^{m\times m\times m} \\
\boldsymbol{A}_{tft} &= \operatorname{spmm}\left(\boldsymbol{E}_t^T, \boldsymbol{A}, \boldsymbol{E}_t\right) \in \mathbb{R}^{m\times m\times m} \\
\boldsymbol{A}_{hft} &= \operatorname{spmm}\left(\boldsymbol{E}_h^T, \boldsymbol{A}, \boldsymbol{E}_t\right) \in \mathbb{R}^{m\times m\times m} \\
\boldsymbol{A}_{tfh} &= \operatorname{spmm}\left(\boldsymbol{E}_t^T, \boldsymbol{A}, \boldsymbol{E}_h\right) \in \mathbb{R}^{m\times m\times m}.
\end{aligned}$$

The resulting adjacency matrices fail to distinguish between loops and paths that go through the same entity multiple times. One way to enable these models to distinguish between closed and open two-paths is to use the full product with masking. For a graphlet $\mathrm{g} = \mathrm{uv_z}$ in the vocabulary $\mathcal{V}_2$ where $\mathrm{u}, \mathrm{v} \in \{\mathrm{f}, \mathrm{r}\}$ and $\mathrm{z} \in \{0, \mathrm{c}\}$ the adjacency matrix is given by $A_{\mathrm{g}} = (a_{\mathrm{g,ij}})_{1\le i,j\le m} \in \mathbb{R}^{m\times m\times|\mathcal{V}_2|}$

$$a_{\mathrm{uv_o,ij}} = \sum_{\substack{l,m,n \\ l\neq m, m\neq n, n\neq l}} \tau(\mathrm{u}, \mathrm{A^i})_{\mathrm{lm}} \cdot \tau(\mathrm{v}, \mathrm{A^j})_{\mathrm{mn}}, \tag{6}$$

$$a_{\mathrm{uv_c,ij}} = \sum_{\substack{l,m \\ l\neq m}} \tau(\mathrm{u}, \mathrm{A^i})_{\mathrm{lm}} \cdot \tau(\mathrm{v}, \mathrm{A^j})_{\mathrm{ml}} \quad \text{with } \mathrm{u}, \mathrm{v} \in \{\mathrm{f}, \mathrm{r}\} \tag{7}$$

where $\tau : \{\mathrm{r}, \mathrm{f}\} \times \mathbb{R}^{n\times n} \to \mathbb{R}^{n\times n}$:

$$\tau(\mathrm{u}, \mathrm{A}) := \begin{cases} A; & \mathrm{u} = \mathrm{f} \\ A^T; & \mathrm{u} = \mathrm{r}. \end{cases}$$

Similar equations hold for longer path.

E.4 SPARQL QUERIES

We display the query patterns for the Vocabularies employed in our Experiments in Tables 18-20

Table 18: 3-Relation Pattern SPARQL Queries correspinding to vocabulary $\mathcal{V}_3$

Pattern	SPARQL Query
fffo	`ASK WHERE { ?e0 {rel1} ?e1 . ?e1 ?rel_0 ?e2 . ?e2 {rel2} ?e3 . FILTER(?e0 != ?e1 && ?e0 != ?e2 && ?e1 != ?e2 && ?e1 != ?e3 && ?e2 != ?e3 && ?e0 != ?e3) }`
fffc	`ASK WHERE { ?e0 {rel1} ?e1 . ?e1 ?rel_0 ?e2 . ?e2 {rel2} ?e0 . FILTER(?e0 != ?e1 && ?e1 != ?e2 && ?e0 != ?e2) }`
ffro	`ASK WHERE { ?e0 {rel1} ?e1 . ?e1 ?rel_0 ?e2 . ?e3 {rel2} ?e2 . FILTER(?e0 != ?e1 && ?e0 != ?e2 && ?e1 != ?e2 && ?e1 != ?e3 && ?e2 != ?e3 && ?e0 != ?e3) }`
ffrc	`ASK WHERE { ?e0 {rel1} ?e1 . ?e1 ?rel_0 ?e2 . ?e0 {rel2} ?e2 . FILTER(?e0 != ?e1 && ?e1 != ?e2 && ?e0 != ?e2) }`
frfo	`ASK WHERE { ?e0 {rel1} ?e1 . ?e2 ?rel_0 ?e1 . ?e2 {rel2} ?e3 . FILTER(?e0 != ?e1 && ?e0 != ?e2 && ?e1 != ?e2 && ?e1 != ?e3 && ?e2 != ?e3 && ?e0 != ?e3) }`

Continued on next page

Table 18 – continued from previous page

Pattern	SPARQL Query
frfc	`ASK WHERE { ?e0 {rel1} ?e1 . ?e2 ?rel_0 ?e1 . ?e2 {rel2} ?e0 . FILTER(?e0 != ?e1 && ?e1 != ?e2 && ?e0 != ?e2) }`
frro	`ASK WHERE { ?e0 {rel1} ?e1 . ?e2 ?rel_0 ?e1 . ?e3 {rel2} ?e2 . FILTER(?e0 != ?e1 && ?e0 != ?e2 && ?e1 != ?e2 && ?e1 != ?e3 && ?e2 != ?e3 && ?e0 != ?e3) }`
frrc	`ASK WHERE { ?e0 {rel1} ?e1 . ?e2 ?rel_0 ?e1 . ?e0 {rel2} ?e2 . FILTER(?e0 != ?e1 && ?e1 != ?e2 && ?e0 != ?e2) }`
rffo	`ASK WHERE { ?e1 {rel1} ?e0 . ?e1 ?rel_0 ?e2 . ?e2 {rel2} ?e3 . FILTER(?e0 != ?e1 && ?e0 != ?e2 && ?e1 != ?e2 && ?e1 != ?e3 && ?e2 != ?e3 && ?e0 != ?e3) }`
rffc	`ASK WHERE { ?e1 {rel1} ?e0 . ?e1 ?rel_0 ?e2 . ?e2 {rel2} ?e0 . FILTER(?e0 != ?e1 && ?e1 != ?e2 && ?e0 != ?e2) }`

Continued on next page

Table 18 – continued from previous page

Pattern	SPARQL Query
rfro	`ASK WHERE { ?e1 {rel1} ?e0 . ?e1 ?rel_0 ?e2 . ?e3 {rel2} ?e2 . FILTER(?e0 != ?e1 && ?e0 != ?e2 && ?e1 != ?e2 && ?e1 != ?e3 && ?e2 != ?e3 && ?e0 != ?e3) }`
rfrc	`ASK WHERE { ?e1 {rel1} ?e0 . ?e1 ?rel_0 ?e2 . ?e0 {rel2} ?e2 . FILTER(?e0 != ?e1 && ?e1 != ?e2 && ?e0 != ?e2) }`
rrfo	`ASK WHERE { ?e1 {rel1} ?e0 . ?e2 ?rel_0 ?e1 . ?e2 {rel2} ?e3 . FILTER(?e0 != ?e1 && ?e0 != ?e2 && ?e1 != ?e2 && ?e1 != ?e3 && ?e2 != ?e3 && ?e0 != ?e3) }`
rrfc	`ASK WHERE { ?e1 {rel1} ?e0 . ?e2 ?rel_0 ?e1 . ?e2 {rel2} ?e0 . FILTER(?e0 != ?e1 && ?e1 != ?e2 && ?e0 != ?e2) }`
rrro	`ASK WHERE { ?e1 {rel1} ?e0 . ?e2 ?rel_0 ?e1 . ?e3 {rel2} ?e2 . FILTER(?e0 != ?e1 && ?e0 != ?e2 && ?e1 != ?e2 && ?e1 != ?e3 && ?e2 != ?e3 && ?e0 != ?e3) }`

Continued on next page

Table 18 – continued from previous page

Pattern	SPARQL Query
rrrc	`ASK WHERE { ?e1 {rel1} ?e0 . ?e2 ?rel_0 ?e1 . ?e0 {rel2} ?e2 . FILTER(?e0 != ?e1 && ?e1 != ?e2 && ?e0 != ?e2) }`

Table 19: 2-Relation Pattern SPARQL Queries corresponding to vocabulary $\mathcal{V}_2$

Pattern	SPARQL Query
ffo	`ASK WHERE { ?e0 {rel1} ?e1 . ?e1 {rel2} ?e2 . FILTER(?e0 != ?e1 && ?e1 != ?e2 && ?e0 != ?e2) }`
ffc	`ASK WHERE { ?e0 {rel1} ?e1 . ?e1 {rel2} ?e0 . FILTER(?e0 != ?e1) }`
fro	`ASK WHERE { ?e0 {rel1} ?e1 . ?e2 {rel2} ?e1 . FILTER(?e0 != ?e1 && ?e1 != ?e2 && ?e0 != ?e2) }`
frc	`ASK WHERE { ?e0 {rel1} ?e1 . ?e0 {rel2} ?e1 . FILTER(?e0 != ?e1) }`
rfo	`ASK WHERE { ?e1 {rel1} ?e0 . ?e1 {rel2} ?e2 . FILTER(?e0 != ?e1 && ?e1 != ?e2 && ?e0 != ?e2) }`

Continued on next page

Table 19 – continued from previous page

Pattern	SPARQL Query
rfc	`ASK WHERE { ?e1 {rel1} ?e0 . ?e1 {rel2} ?e0 . FILTER(?e0 != ?e1) }`
rro	`ASK WHERE { ?e1 {rel1} ?e0 . ?e2 {rel2} ?e1 . FILTER(?e0 != ?e1 && ?e1 != ?e2 && ?e0 != ?e2) }`
rrc	`ASK WHERE { ?e1 {rel1} ?e0 . ?e0 {rel2} ?e1 . FILTER(?e0 != ?e1) }`

Table 20: N-M Pattern SPARQL Queries corresponding to vocabulary $\mathcal{V}_{\bullet}^{+}$

Pattern	SPARQL Query
ffo_1-2	`ASK WHERE { ?e0 {rel1} ?e1 . ?e1 {rel2} ?e2 . ?e1 {rel2} ?e3 . FILTER(?e0 != ?e1 && ?e1 != ?e2 && ?e2 != ?e3 && ?e3 != ?e0 && ?e0 != ?e2 && ?e1 != ?e2) }`
fro_1-2	`ASK WHERE { ?e0 {rel1} ?e1 . ?e2 {rel2} ?e1 . ?e3 {rel2} ?e1 . FILTER(?e0 != ?e1 && ?e1 != ?e2 && ?e2 != ?e3 && ?e3 != ?e0 && ?e0 != ?e2 && ?e1 != ?e2) }`

Continued on next page

Table 20 – continued from previous page

Pattern	SPARQL Query
rfo_1-2	`ASK WHERE { ?e1 {rel1} ?e0 . ?e1 {rel2} ?e2 . ?e1 {rel2} ?e3 . FILTER(?e0 != ?e1 && ?e1 != ?e2 && ?e2 != ?e3 && ?e3 != ?e0 && ?e0 != ?e2 && ?e1 != ?e2) }`
rro_1-2	`ASK WHERE { ?e1 {rel1} ?e0 . ?e2 {rel2} ?e1 . ?e3 {rel2} ?e1 . FILTER(?e0 != ?e1 && ?e1 != ?e2 && ?e2 != ?e3 && ?e3 != ?e0 && ?e0 != ?e2 && ?e1 != ?e2) }`
ffo_2-2	`ASK WHERE { ?e0 {rel1} ?e2 . ?e1 {rel1} ?e2 . ?e2 {rel2} ?e3 . ?e2 {rel2} ?e4 . FILTER(?e0 != ?e1 && ?e1 != ?e2 && ?e2 != ?e3 && ?e3 != ?e0 && ?e0 != ?e2 && ?e1 != ?e2 && ?e4 != ?e0 && ?e4 != ?e1 && ?e4 != ?e2 && ?e4 != ?e3) }`
fro_2-2	`ASK WHERE { ?e0 {rel1} ?e2 . ?e1 {rel1} ?e2 . ?e3 {rel2} ?e2 . ?e4 {rel2} ?e2 . FILTER(?e0 != ?e1 && ?e1 != ?e2 && ?e2 != ?e3 && ?e3 != ?e0 && ?e0 != ?e2 && ?e1 != ?e2 && ?e4 != ?e0 && ?e4 != ?e1 && ?e4 != ?e2 && ?e4 != ?e3) }`

Continued on next page

Table 20 – continued from previous page

Pattern	SPARQL Query
rfo_2-2	`ASK WHERE { ?e2 {rel1} ?e0 . ?e2 {rel1} ?e1 . ?e2 {rel2} ?e3 . ?e2 {rel2} ?e4 . FILTER(?e0 != ?e1 && ?e1 != ?e2 && ?e2 != ?e3 && ?e3 != ?e0 && ?e0 != ?e2 && ?e1 != ?e2 && ?e4 != ?e0 && ?e4 != ?e1 && ?e4 != ?e2 && ?e4 != ?e3) }`
rro_2-2	`ASK WHERE { ?e2 {rel1} ?e0 . ?e2 {rel1} ?e1 . ?e3 {rel2} ?e2 . ?e4 {rel2} ?e2 . FILTER(?e0 != ?e1 && ?e1 != ?e2 && ?e2 != ?e3 && ?e3 != ?e0 && ?e0 != ?e2 && ?e1 != ?e2 && ?e4 != ?e0 && ?e4 != ?e1 && ?e4 != ?e2 && ?e4 != ?e3) }`